PB-213 263

PORTABLE LASER VELOCIMETER FOR STACK VELOCITY MEASUREMENTS

L. O. Heflinger, et al

TRW Systems Group

Prepared for:

Environmental Protection Agency

November 1972

DISTRIBUTED BY:

NTIS

National Technical Information Service
U. S. DEPARTMENT OF COMMERCE
5285 Port Royal Road, Springfield Va. 22151

EPA-R2-72-132

TRW REPORT NO. 20852-6002-R0-00

PB 213 263

FINAL REPORT

PORTABLE LASER VELOCIMETER FOR STACK VELOCITY MEASUREMENTS

NOVEMBER 1972

Prepared by

L.O. HEFLINGER, B.J. MATTHEWS, and H. SHELTON

Prepared for

ENVIRONMENTAL PROTECTION AGENCY
RESEARCH TRIANGLE PARK, NORTH CAROLINA

TRW SYSTEMS GROUP

ONE SPACE PARK • REDONDO BEACH • CALIFORNIA

Reproduced by
NATIONAL TECHNICAL
INFORMATION SERVICE
U S Department of Commerce
Springfield VA 22151

68

BIBLIOGRAPHIC DATA SHEET	1. Report No. EPA-R2-72-132	2.	3. Recipient's Accession No. PB-213 263
4. Title and Subtitle: Portable Laser Velocimeter for Stack Velocity Measurements			5. Report Date: November 1972 6.
7. Author(s): L.O. Heflinger, B.J. Matthews, and H. Shelton			8. Performing Organization Rept. No. 20852-6002-RO-00
9. Performing Organization Name and Address: TRW Systems Group One Space Park Redondo Beach, California			10. Project/Task/Work Unit No. 11. Contract/Grant No. 68-02-0308
12. Sponsoring Organization Name and Address: ENVIRONMENTAL PROTECTION AGENCY Research Triangle Park, North Carolina 27711			13. Type of Report & Period Covered: Final 14.

15. Supplementary Notes

16. Abstracts

The report describes the design and development of a short range, laser velocimeter together with the analysis of optical velocity measurement techniques over ranges up to 1500 ft. This laser velocimeter operates on an interference-backscatter principle. It is portable and designed to measure velocities of flowing particle laden gases in power plant ducts or stacks at relatively close ranges. The instrument is composed of a sensing head cabinet and an electronics cabinet. The sensing head incorporates a laser illuminator, beam forming optics and photodetector. The electronics cabinet contains a signal processing circuit, spectrum analyzer, and power supplies for the laser and spectrum analyzer. The design, construction and preliminary testing of the velocimeter are discussed in Section 2. Section 3 discusses the analysis of optical velocity measuring devices for extended range operation. Three types of optical velocimeters were considered: Doppler shift; interference-fringe; and a reticle velocimeter.

17. Key Words and Document Analysis. 17a. Descriptors

Air pollution
Measurement
Flue gases
Velocity measurement
Speed indicators
Lasers
Portable equipment
Optical properties
Design
Doppler shift
Reticles

Details of illustrations in this document may be better studied on microfiche.

17b. Identifiers/Open-Ended Terms

Air pollution detection
Interference-fringe

17c. COSATI Field/Group 13B Ia

18. Availability Statement	19. Security Class (This Report)	21. No. of Pages
Unlimited	UNCLASSIFIED	76 68
	20. Security Class (This Page) UNCLASSIFIED	22. Price 3.00

TRW REPORT NO. 20852-6002-R0-00

FINAL REPORT

PORTABLE LASER VELOCIMETER FOR STACK VELOCITY MEASUREMENTS

NOVEMBER 1972

Prepared by

L.O. HEFLINGER, B.J. MATTHEWS, and H. SHELTON

Prepared for

ENVIRONMENTAL PROTECTION AGENCY
RESEARCH TRIANGLE PARK, NORTH CAROLINA

TRW SYSTEMS GROUP

ONE SPACE PARK • REDONDO BEACH • CALIFORNIA

CONTENTS

		Page
1.	INTRODUCTION AND SUMMARY	1
2.	PORTABLE LASER VELOCIMETER	3
2.1	Background	3
2.2	Velocimeter Operating Principle	5
2.3	Velocimeter Optical System	6
2.4	Velocimeter Electronics	13
2.5	Velocimeter Testing	22
3.	LONG RANGE OPTICAL VELOCITY METERS	28
3.1	Introduction	28
3.2	Smoke Optical Properties	31
3.3	Sample Volume Size	32
3.4	Significance of the Smoke Optical Properties in Conjunction with the Sample Volume Size	35
3.5	Shot Noise of Detection	36
3.6	The Direct Doppler System	38
3.7	The Fringe Velocimeter: Granularity Noise	42
3.8	Fringe Velocimeter: Required Laser Power	48
3.9	Reticle Velocimeter Noise Estimate	51
3.10	Preliminary Experiments with a Reticle Velocimeter	53
4.	CONCLUSIONS	55
4.1	Portable Laser Velocimeter	55
4.2	Long Range Velocimeters	55
	REFERENCES	57
	APPENDICES	
A	SPECIFICATIONS FOR SPECTRA-PHYSICS MODEL 120 GAS LASER WITH MODEL 256 EXCITER	58
B	LASER VELOCIMETER DRAWING LIST	59

Preceding page blank

ILLUSTRATIONS

		Page
1.	Velocimeter electronics cabinet and sensing head	1
2.	Schematic of the interference between two coherent light beams	4
3.	Schematic diagram of laser velocimeter optical system	7
4.	Laser velocimeter sensing head assembly	10
5.	Photograph of velocimeter sensing head showing component placement	11
6.	Photograph of velocimeter sensing head showing framework and controls	12
7.	Three-quarter view of sensing head	13
8.	Oscilloscope traces of PMT signals at the output of the bandpass amplifier in the breadboard velocimeter	15
9.	Oscilloscope traces of spectrum analyzer signals obtained with the breadboard velocimeter	17
10.	Electronic circuit diagram for the laser velocimeter	19
11.	Laser velocimeter sensing head	23
12.	Velocimeter electronics package	23
13.	Plot of measured versus calculated velocity for laser velocimeter	24
14.	Air and predicted particle (droplet) velocity	27
15.	Direct doppler velocity meter	28
16.	Schematic of fringe velocimeter	29
17.	Reticle velocimeter	30
18.	Beam intersection geometry	33
19.	Effect of turbulence on direct doppler system	38
20.	Granularity noise in the fringe velocimeter	42

Preceding page blank

FOREWORD

This report summarizes work done under Environmental Protection Agency Contract No. 68-02-0308, dated 30 June 1971. Activities under this contract were concerned with: (1) design and construction of a portable laser velocimeter for stack velocity measurements at close range; and (2) analysis of optical velocity measurement techniques over ranges up to 1500 feet.

Technical direction and administration of this project by the Environmental Protection Agency was provided by Dr. Frederic C. Jaye. The TRW Project Manager was Mr. Birch J. Matthews. Drs. Haywood Shelton and Lee O. Heflinger developed the laser velocimeter instrument and the analysis for extended range use of optical velocity meters, respectively.

The authors wish to thank Mr. William F. Daley for his valuable assistance in the design and fabrication of the laser velocimeter. Mr. Robert F. Kemp also made significant contributions to the initial design concepts for the optical and electronic systems.

Preceding page blank

1. INTRODUCTION AND SUMMARY

This report describes the design-development of a short range laser velocimeter together with an analysis of potential extended range optical velocity measuring techniques. The work was done under contract to the Environmental Protection Agency.

The laser velocimeter constructed during this program operates on an interference-backscatter principle. It is portable and designed to measure velocities of flowing particle laden gases in power plant ducts or stacks at relatively close ranges. The instrument is composed of a sensing head cabinet and an electronics cabinet. These are pictured in Figure 1. The

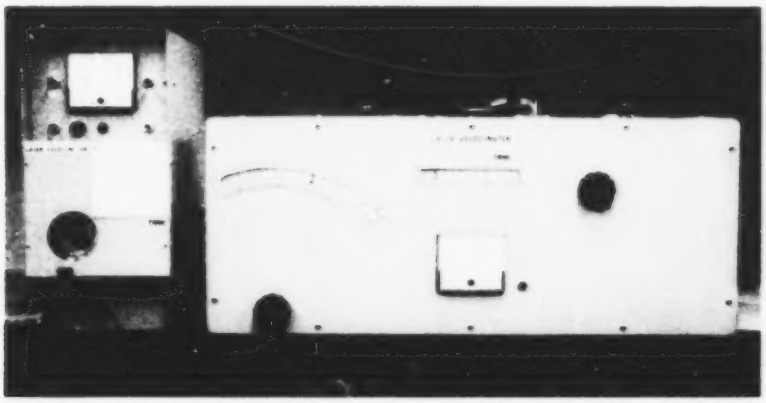

Figure 1. Velocimeter electronics cabinet (l) and sensing head (r).

sensing head incorporates a laser illuminator, beam forming optics and photodetector. The electronics cabinet contains a signal processing circuit, spectrum analyzer, as well as power supplies for the laser and spectrum analyzer. The spectrum analyzer is used to analyze the frequency signals generated by the sensing head. Following are design and operating characteristics for this laser velocimeter:

- Velocity sensing range - 10 to 125 ft/sec
- Focal length range - 2 to 15 ft
- Measuring medium - Fossil fuel stack gas
- Sensing head weight - 25 lb
- Sensing head envelope - 27-3/4 x 11-3/4 x 6-7/8 inches
- Electronics weight - 25 lb
- Electronics envelope - 12-1/2 x 16 x 7-1/4 inches
- Readout * (Meter) - Mean velocity, ft/sec
  20 sec. time constant
- Readout (meter) - Velocity deviation, ft/sec
  5 sec time constant
- Power requirements - 110v, 60 Hz, <5 amp

The design, construction and preliminary testing of this velocimeter are discussed in Section 2.

The second major program task was an analysis of optical velocity measuring devices for extended range operation. Of interest here was remote stack plume velocity measurements over distances of 300 to 1500 feet. Three types of optical velocimeters were considered; namely, Doppler shift, interference-fringe, and a reticle velocimeter. This discussion is presented in Section 3.

* 0-100 mv analog signal available.

2. PORTABLE LASER VELOCIMETER

2.1 BACKGROUND

When two coherent beams of light intersect in space, stationary three-dimensional interference fringe patterns are established. The fringe spacing Δ is a function of the wavelength of light λ and the angle θ at which the two beams intersect. This is shown in Figure 2. In this illustration, both beams are parallel beams of light, as though from point sources at infinity. Each is traveling at the velocity of light C, each is of wavelength λ, and both are coherent to each other. The two beams of light pass through each other at an angle θ. Since light is a transverse electromagnetic phenomenon, the direction of vibration of the electric component is perpendicular to the plane of the drawing. For plane waves, the electric intensity varies sinusoidally in strength as one moves down the wave train.

The wavelength λ is the physical separation between adjacent maxima of the traveling electric field. When the maxima of one wave are superimposed on the maxima of another, the amplitudes add, constructively. When the maxima of one wave are superimposed with the minima of the other, the two destructively interfere. If the wavefronts are of equal amplitude, the net amplitude is zero at these points. The loci of constructive interference trace out the straight lines shown in Figure 2. In the case of beams of finite cross section, planes are actually traced out. These planes, or alternate lines of darkness and light, are parallel to the bisector of the angle θ between the direction of propagation of the two beams. The regions of destructive interference form periodic planes of absolute darkness. In Figure 2, the loci of constructive interference are indicated by the parallel lines (regions of light). Destructive interferences are the blank regions (no light)

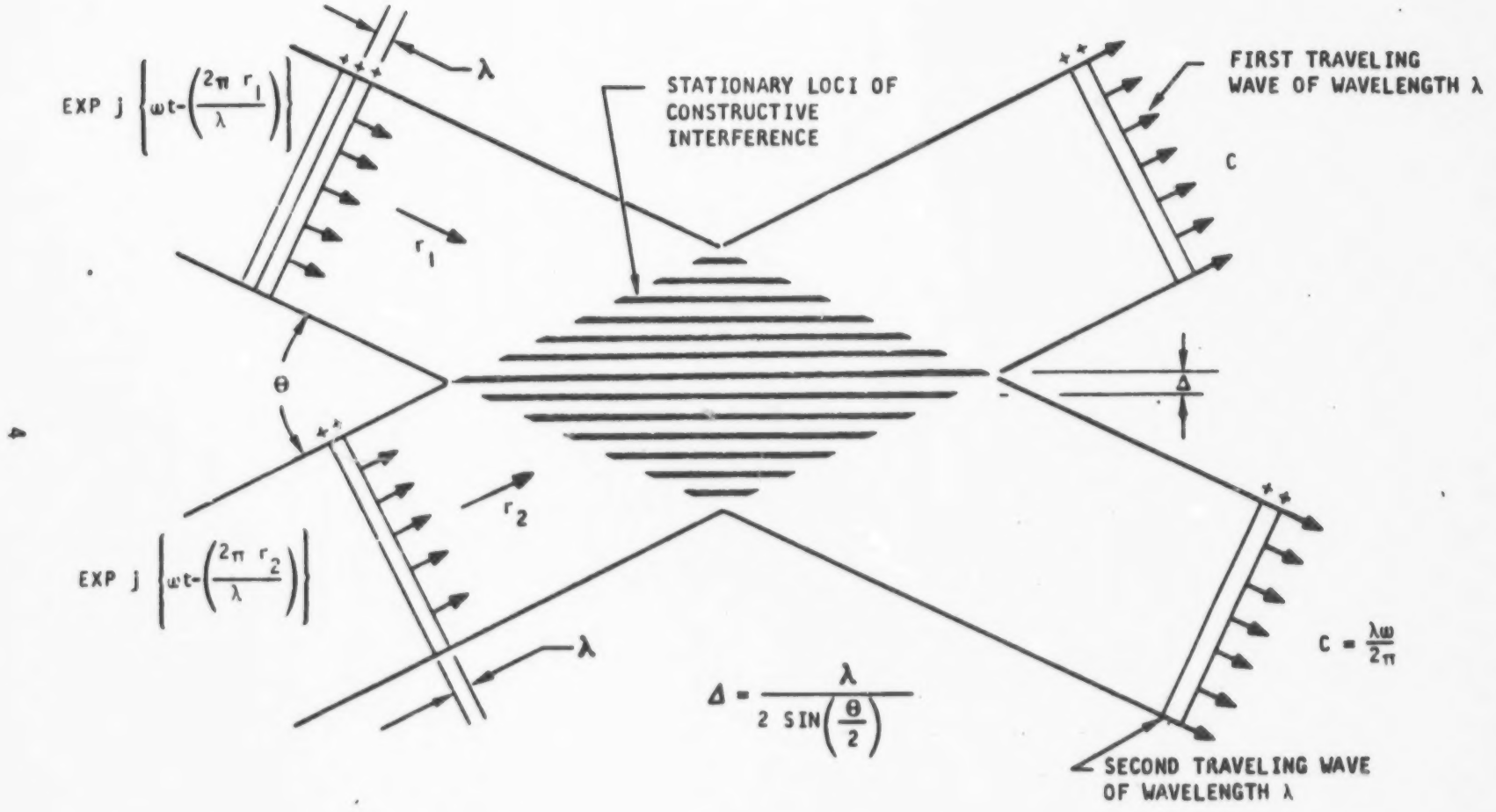

Figure 2. Schematic of the interference between two traveling collimated coherent beams of light of wavelength λ passing through each other at an angle of θ.

in between. Neighboring dark or light regions are separated by a distance

$$\Delta = \frac{\lambda}{2 \sin \theta/2}$$

As an example, when the two beams pass through one another at an angle of 60 degrees, the loci of constructive interference are separated from each other by the wavelength of light. Deep red light has a wavelength of 0.7 micron or 27.5 microinches.

2.2 VELOCIMETER OPERATING PRINCIPLE

The laser velocimeter described subsequently utilizes the wave interference properties of two coherent light beams described in the previous section. Two beams (<1 mm diameter) of coherent light derived from a helium-neon gas laser (λ=0.6328μ) intersect in space establishing an interference fringe pattern. The beams intersect at an angle of approximately 1 degree (1/60 radian). Horizontal fringe spacing is 0.0015 inch in an intersection volume about 1/2 mm wide and 1 cm long.

Particulate laden combustion gas passes through the region of interference. A particle moving through adjacent fringes of constant separation will scatter light periodically. If this scattered light is collected and focused onto a photodetector, it will produce a coincident pulsating electric current whose frequency is proportional to the particle's velocity. In the present velocimeter system, the frequency of light modulation ranges from 80 Kc to 1 Mc corresponding to a velocity range of 10 to 125 ft/sec.

The output of the photodetector is fed into a spectrum analyzer which is a sensitive receiver that can be electronically swept from near zero frequency to above 1 megacycle. The input frequency is indicated by the value of the sweep voltage at the instant an output signal is obtained. The value of this voltage is stored and displayed on a meter and read as the proportional velocity. The velocimeter

electronic circuit will search for a lock on any frequency of sufficient amplitude which is present.

2.3 VELOCIMETER OPTICAL SYSTEM

The laser velocimeter is a single station instrument requiring only one port or opening in the power plant stack. The signals received by the optical system are those generated by low angle particulate scattering in the backward direction.

The optical system is self-aligning which automatically focuses the two coherent light beams to a crossover point in space. The same optics collect the backscatter and focus it onto a photodetector. A schematic of the velocimeter optical arrangement is shown in Figure 3.

The illumination source is a Spectra-Physics helium-neon gas laser which emits 5 mw power at $\lambda = 0.6328\mu$(red light)*. Specifications for this laser are provided in Appendix A.

This laser was selected on the basis of reliability, plasma tube life, ruggedness and maximum power output consistent with size and weight limitations.

From the schematic of Figure 3, it will be seen that the optical path is folded to obtain a compact design. Collimated light from the continuous wave helium-neon laser is incident on an adjustable-beam

---

* Spectra-Physics Model 120 Gas Laser with Model 256 Exciter. Product of Spectra-Physics, Inc., 1250 West Middlefield Road, Mountain View, California.

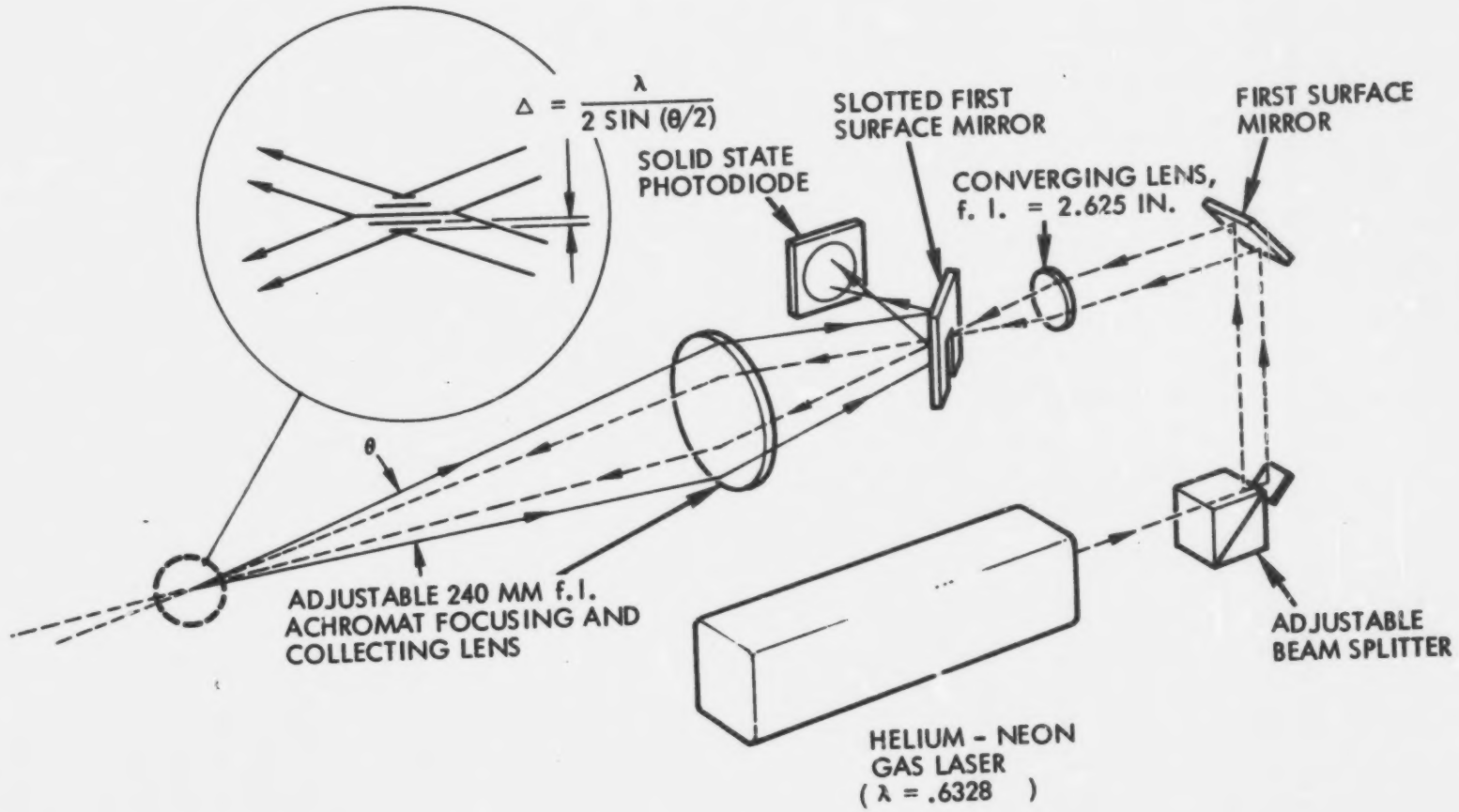
Δ = λ / 2 SIN (θ/2)
SOLID STATE PHOTODIODE
SLOTTED FIRST SURFACE MIRROR
CONVERGING LENS, f. l. = 2.625 IN.
FIRST SURFACE MIRROR
θ
ADJUSTABLE 240 MM f.l. ACHROMAT FOCUSING AND COLLECTING LENS
ADJUSTABLE BEAM SPLITTER
HELIUM - NEON GAS LASER (λ = .6328)

Figure 3. Schematic diagram of laser velocimeter optical system.

splitter. The beam splitter consists of back-to-back 90-degree prisms. The two-prism interface transmits 50 percent of the beam onto a small first surface mirror mounted at 45 degrees to the incident beam. The coated prism interface reflects the other 50 percent of the primary beam parallel to the transmitted beam. The prism assembly and small first surface mirror move in pure translation with respect to each other about a common centerline thus providing adjustable and parallel beam separation. Beam separation ranges from a minimum of 0.062 in. to 0.80 in. This range of beam separation allows a constant separation of the stationary fringe pattern in space of approximately 40 microns.

After division, the parallel beams are turned 90 degrees by a second first surface mirror and made parallel to the optical axis of the telescope. The beams are converged to a focal point by a 2.625 in focal length lens. After crossover, the beams diverge and pass through a 0.062 in. split first surface mirror assembly. The split mirror passes the diverging beams through to a focusing 240 mm focal length achromat lens. This 4.332-inch diameter lens causes the two parallel beams to converge in space. The achromat lens telescopes through a distance of 5.50 inches providing a beam crossover location in space from 2 to 15 feet along the optical axis. Movement of the achromat lens holder is accomplished with a rack and pinion gear assembly. Fringe spacing is held constant by manually adjusting the lens travel and beam splitter to previously calibrated positions.

Backscattered light by particulate in the flowing gas passing through the stationary interference pattern is collected by the achromat lens and reflected by the split first surface mirror assembly. This mirror, mounted at 45 degrees to the optical axis, allows the scattered light to be focused at an aperture located before a photodetector. With the exception of the traveling achromat lens, all components of the optical system are precisely and rigidly mounted to insure that the scattered lignt is brought to focus before the photodetector.

Figure 4 is a layout drawing of the laser velocimeter sensing head. This drawing shows the placement of the gas laser chassis and critical optical components. A tabulation of the sensing head detail drawings is presented in Appendix B. The photographs in Figures 5 through 7 illustrate the basic construction and optical component placement of the sensing head. With the exception of the traveling objective lens, all of the beam forming optics are mounted on one rigid platform to preserve alignment. The alignment of the objective lens is not as critical because the system is self-aligning with respect to its movement.

In adapting the laser to the sensing head, the outer case was removed (to save weight) and mounting holes machined in the laser chassis.* The front end of the laser is rigidly mounted to the optical platform. A single point pin mount parallel to the optical axis is used at the other end to permit thermal expansion of the laser chassis.

The laser and critical beam forming components on the optical platform are mounted to a 1/2 inch aluminum angle frame at three points. An aluminum sheet metal cover enclosing the optics is attached to the frame. The three point tie-down of the optics is designed to minimize any optical path misalignment due to external forces applied to the frame or cover.

The basic design concept for the sensing head optical system was predetermined by the requirement for an interference-backscatter instrument. This being the case, sensing head design was limited to compact packaging and maintenance of optical path considerations. More attention, however, was given to selection of a suitable photodetector and design of signal processing electronics. These subjects are discussed in the section following.

---

* TRW Drawing No. SK 1038-12.

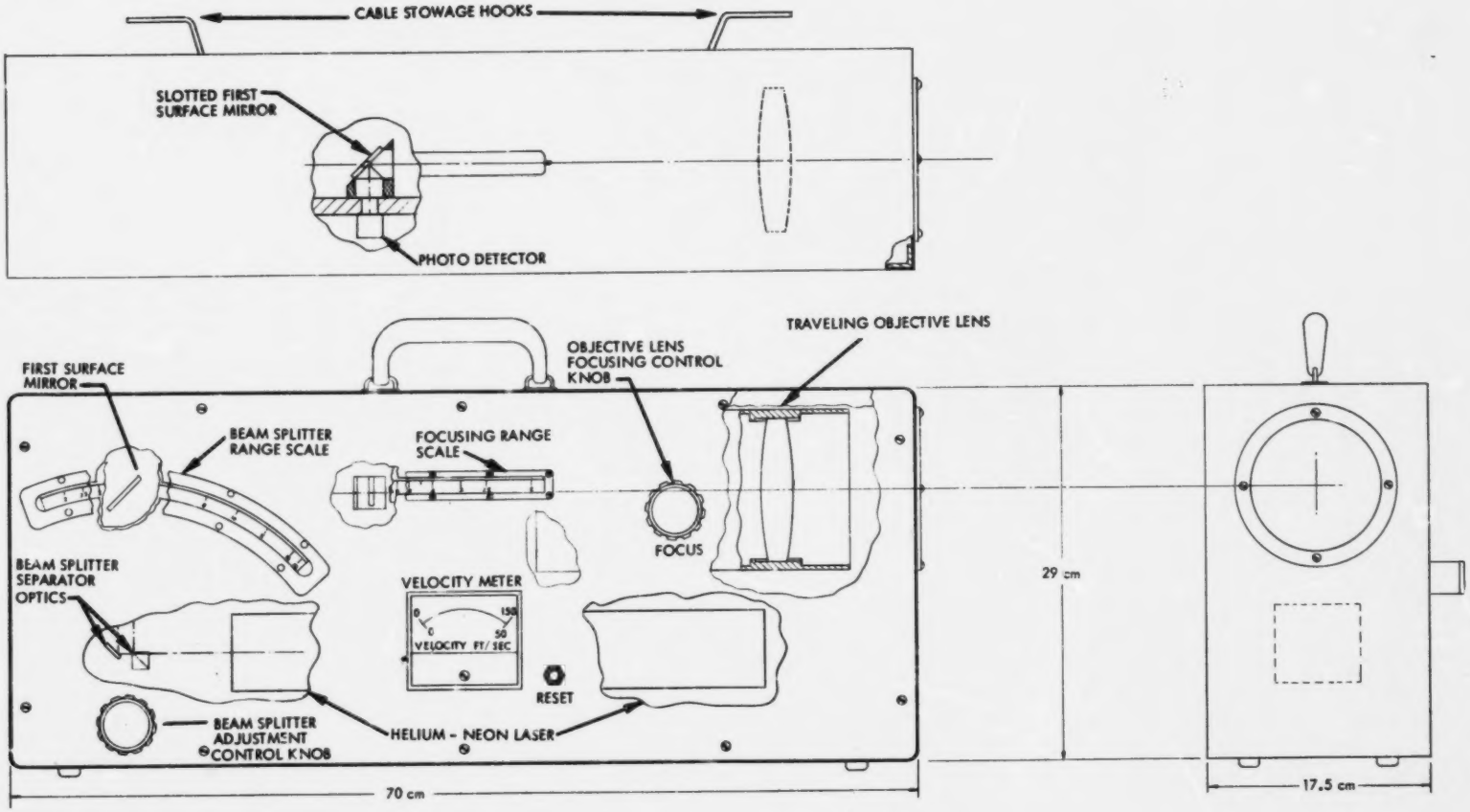

Figure 4. Laser velocimeter sensing head assembly.

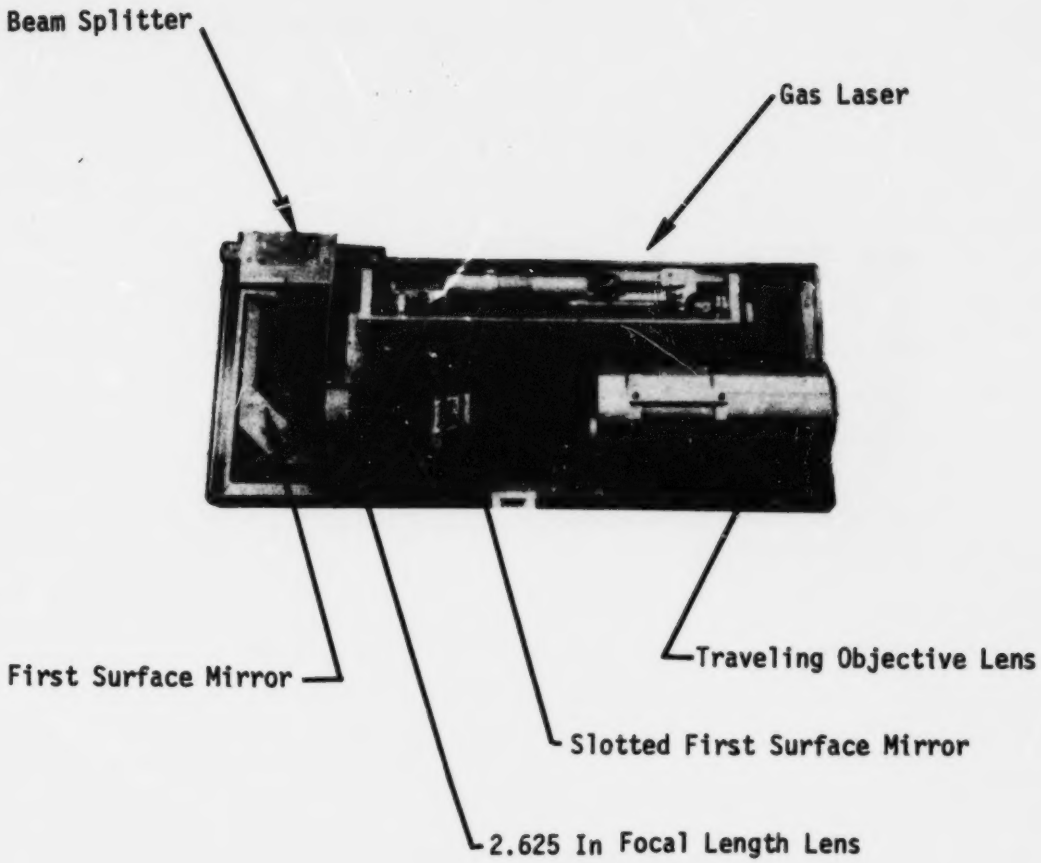

Figure 5. Photograph of the laser velocimeter sensing head assembly showing the placement of the various components.

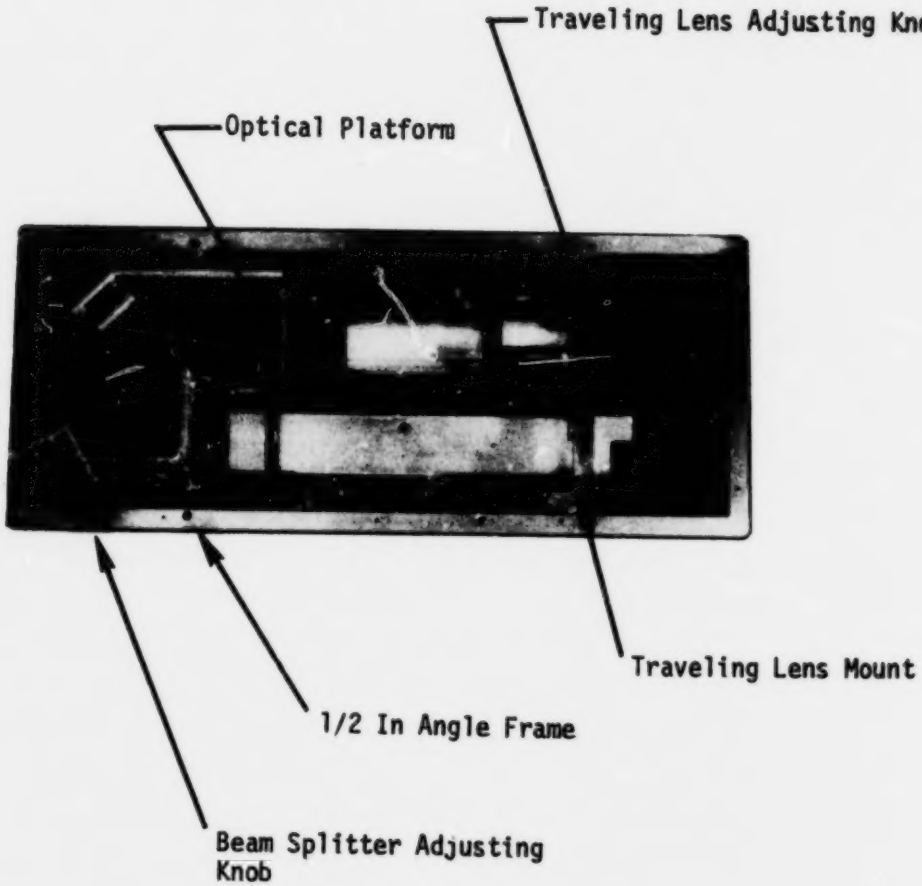

Figure 6. Photograph of the other side of the sensing head assembly showing the location of the two control knobs used to focus the adjustable beam splitter and traveling objective lens.

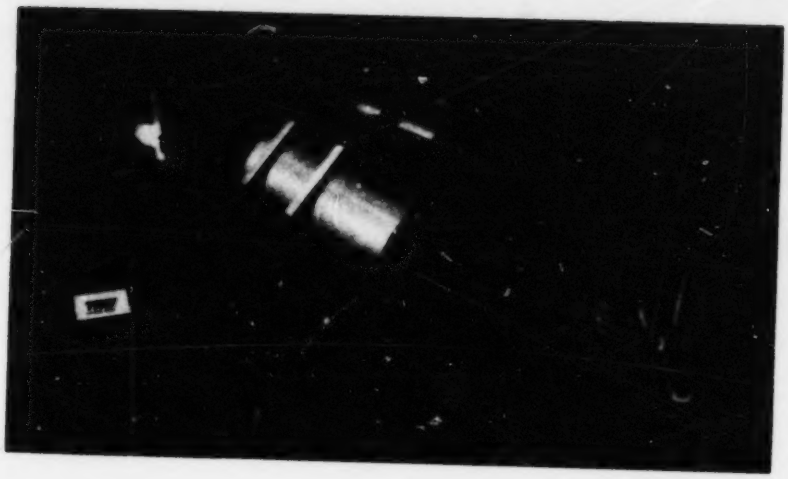

Figure 7. Three-quarter view of the sensing head. The focusing lens and cylindrical housing are shown in the foreground of the photograph.

2.4 VELOCIMETER ELECTRONICS

In describing the optical system, it was noted that an adjustable beam splitter is used to maintain constant fringe spacing within the limits of the objective lens travel. A fixed beam splitter arrangement was considered. Such an arrangement (variable fringe spacing), results in excessively high frequency signals at short range; extended sampling (beam crossover) volumes at long range; and, more sophisticated signal processing electronics. For these reasons, the fixed beam splitter design approach was not adopted in the present design.

Initial work on the velocimeter electronics centered on selection of a photodetector and signal processing system. A survey of readily available photomultiplier tubes (PMT) and solid state diodes was made. A type 4473 PMT and a type MRD 500 silicon photo diode were selected as candidates. The type 4473 PMT is structurally similar to types 931, 1P28 and 1P21 and is, in effect, a 1P21 selected for maximum "red" sensitivity. The MRD 500 photo diode has a spectral range

throughout the visible and near-infrared.* Peak sensitivity for this diode is about 0.8 micron. Response time is typically <1 nanosecond.

A laboratory breadboard velocimeter system was set-up for the purpose of generating typical electrical signals. This set-up consisted of a 3 mw helium-neon gas laser, a beam splitter, simple positive lens, a slotted first surface mirror, pinhole and PMT assembly, and a 10-inch focal length, f/5 achromatic objective lens. The optical arrangement was, in concept, the same as that shown in Figure 3. A photomultiplier power supply and bandpass amplifier were used with the PMT.

A moving target (smoke simulator) was devised by cutting a circular groove in a plexiglas disk. A mixture of flyash and coil dope was poured into the groove and allowed to dry. When rotated by a small motor, the disk made a useful target for the velocimeter and was capable of generating known constant or variable velocities within the design range of the instrument.

The oscilloscope photographs of Figure 8 show traces of a 1P28 PMT signal at the output of the bandpass amplifier in the breadboard velocimeter system. These were obtained from the spinning disk. At a sweep speed of 5 msec/div, Figure 8 shows a large number of spikes, resulting from point-to-point differences in scattering properties or in the number of scattering particles in the laser beam at any one time. The density of particles on the rotating track was intended to represent a relatively light loading (approximately 1 grain/ft^3) in a gas stream.

In Figure 8a, the spikes are nearly symmetrical about the zero axis. The bandpass amplifier used transmitted frequencies between

---

* Product of Motorola Semiconductor Products, Inc., Type MRD 500 P-I-N Silicon Photo Diode.

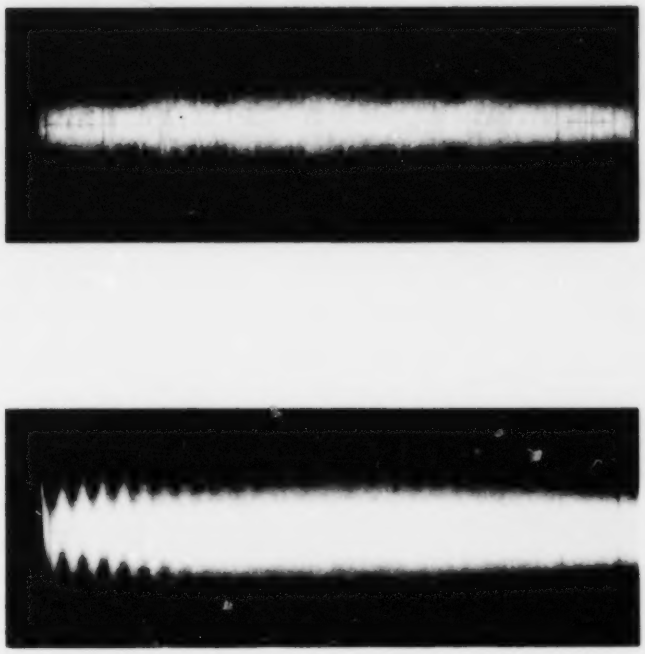

(b)

Figure 8. Photomultiplier tube signals at the output of the bandpass amplifier in the breadboard laser velocimeter. The upper figure is at a sweep rate of 5 msec/division and shows scattering from clumps of particles. The lower figure gives an indication of the autocorrelation of the signal at the frequency of the velocity-generated signal (about 140 kHz).

about 30 kHz and 600 kHz. At higher sweep speeds, most of the spikes are seen to contain strong component signals at the laser doppler frequency corresponding to the velocity of the track. Figure 8b is a composite of many such traces taken with the oscilloscope trigger level set to show synchronization with the velocity signal at about 140 kHz. After 9 or 10 cycles, the signal appears to merge into the statistical noise in the phototube signal; however, close inspection of the original photograph revealed a faint but persistent component of this signal throughout the trace. The task of detecting this signal, therefore, becomes one of deriving an intermittent signal out of a comparable amount of noise.

Following these preliminary breadboard tests, consideration was next given to the means by which the photodetector signal would be processed. A wide variety of signal processor systems have been used with laser doppler velocimeters. Of these, three types were used with the breadboard optical system. Attempts were made to measure the doppler frequency directly with frequency counters and also with a pulse-averaging wide-band discriminator. An attempt was also made to use the frequency counter in a period-averaging mode. Finally, the signals were examined with a spectrum analyzer. It quickly became clear that for the first of these methods to work, considerable pre-processing of the signals would be required ahead of the counter or discriminator.

A basic problem with the direct-measuring methods is the matter of signal continuity. If the velocity signal were completely continuous, the appropriate readout device would most nearly resemble a frequency-modulation radio receiver having an indicating meter instead of the audio circuits. With discontinuous signals, simple burst counting methods will work, provided bursts are of sufficient length to be processed after they are recognized. A fairly elaborate burst pre-processor for use with sparsely seeded gas streams has been described by Lennert, et. al.[1] The spectrum analyzer, on the other hand, processes all signals, and leaves the problem of recognition to be dealt with as a subsequent step.

A wide-band spectrum analyzer* shows that the signal from the PMT (Figure 8) contains a nearly constant level of noise within the bandpass of the instrument together with a recognizable signal at the laser doppler frequency. Figure 9 is a photograph of a (selected) single sweep of the spectrum analyzer through the range of 8 kHz to about 300 kHz showing a recognizable signal at about 140 kHz. All sweeps do

* Tektronix Type 1L5, Plug-In Unit.

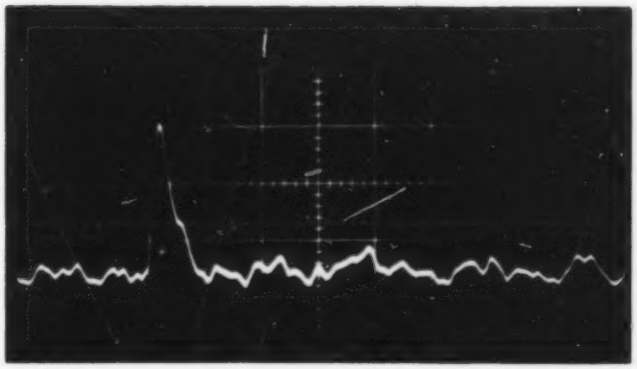

(a)

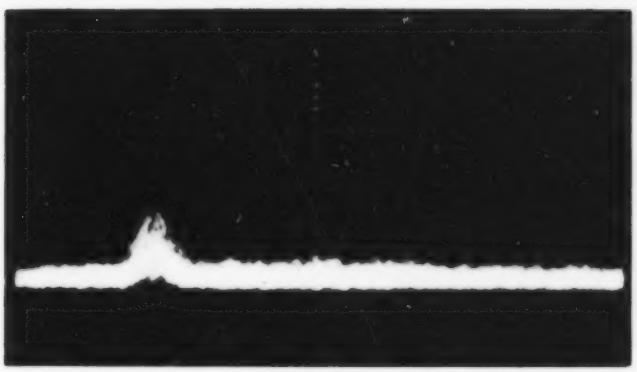

(b)

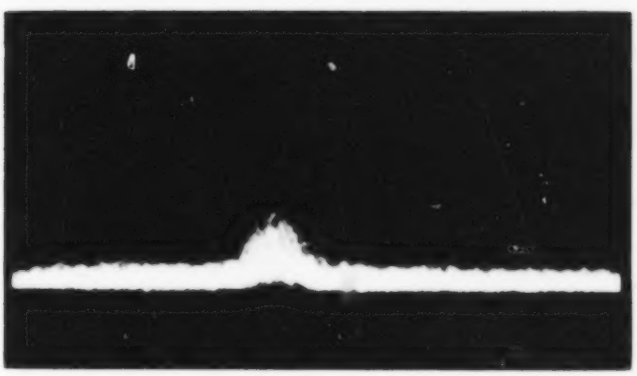

(c)

Figure 9. Spectrum analyzer signals obtained with the breadboard velocimeter. The upper trace is a single sweep showing an especially strong pulse. The other traces are composites of about 250 sweeps each showing peaks at 140 kHz and 210 kHz, respectively.

not have the same signal to noise ratio; a strong signal such as this represents a coincidence between the spectrum analyzer local oscillator and the passage of a particularly reflective particle through the laser beam intersection volume. Figures 9b and 9c are composites of about 250 such traces each with the rotational speed of the target wheel set to generate signals of 140 kHz and 210 kHz, respectively. Nearly all of these traces produce pulses which can be recognized by a level detector set, for example, at the second major division from the bottom.

These results suggested that a velocimeter instrument having the greatest versatility could best be made by using a spectrum analyzer as the primary signal processor. It would, in effect, continuously scan the range of the instrument (or a selected portion of the total range) for recognizable signals.

A silicon photo diode was next acquired and evaluated. Use of a solid state photodetector offered several potential advantages. The efficiency of the MRD 500 diode in converting incident photons (at the laser wavelength $=0.6328\mu$) to electrons is near unity. Correspondingly, the quantum efficiencies for PMT's is typically 2 to 3 percent. Further, the diode offered the desirable feature of being compact and rugged. And finally, the signal-to-noise ratio for the photo diode and photo diode circuit appeared superior in testing (at $\lambda=0.6328\mu$) to comparable PMT systems.

These arguments led to design of a photo diode circuit and incorporation of a Tektronix 1L5 spectrum analyzer for signal processing. The resulting electronics circuit is shown in the Figure 10 schematic.

The Motorola photo diode has a back leakage current proportional to the light falling on it. Its current flows through a 47 kΩ register and a bipassed monitor resistance (so the current can be peaked for

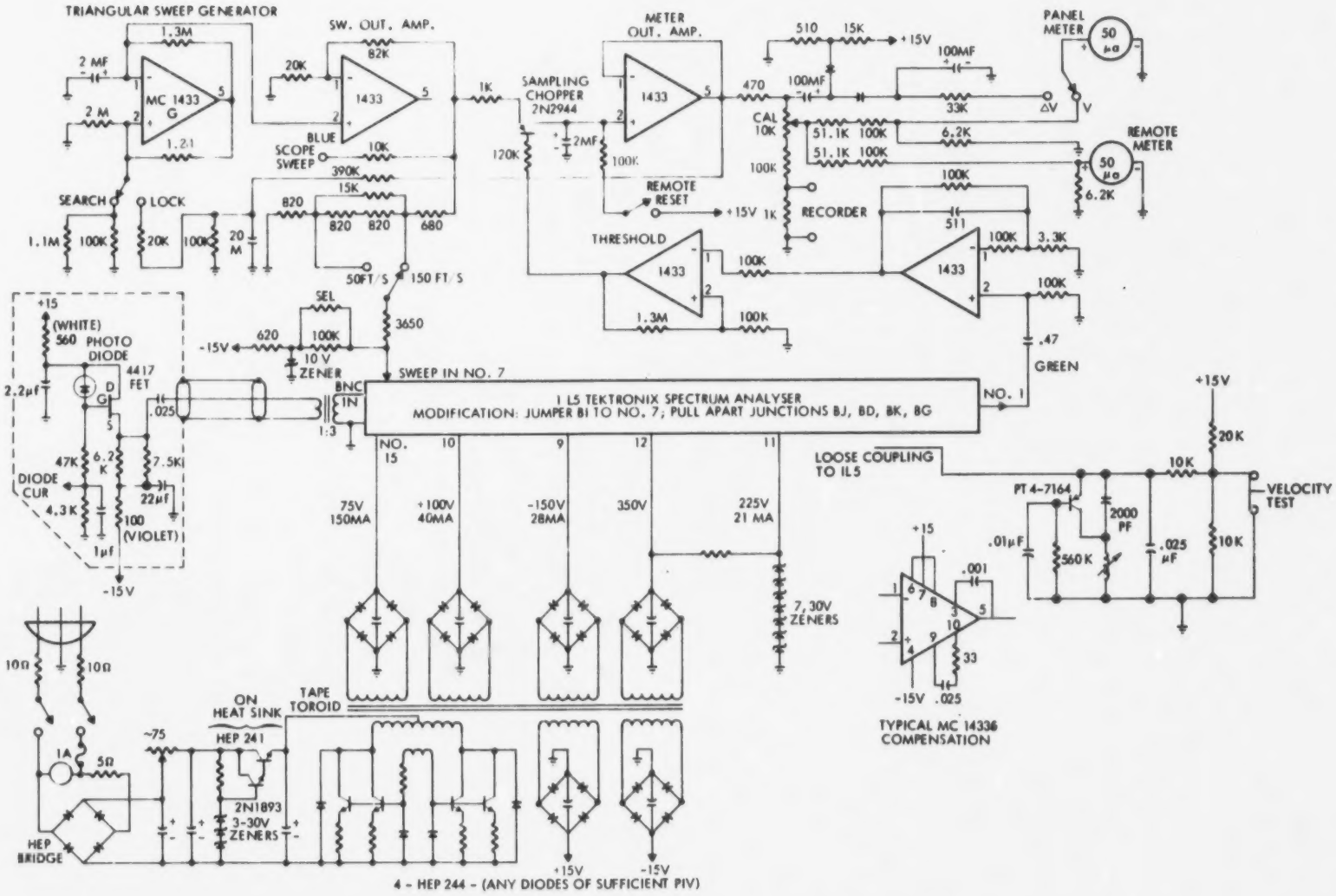

Figure 10. Electronic circuit diagram for the laser velocimeter.

alignment purposes). This resistance and the shunt capacity (~4 pf) give a 3 db high frequency attenuating at about 1 mc. The voltage across this resistor is led to the gate of a 2N4417 Field-effect transistor operating as a source-follower to drive the capacity of the coaxial which leads to a 3:1 step up transformer. This series capacity and shunt inductance give a low frequency cut-off at about 60 kc. High frequency response is about 1 mc with the input capacity of the spectrum analyzer and cable.

The 1L5 spectrum analyzer is modified as shown on the Figure 10 schematic so as to require least power, to functionally eliminate many of the analyzer control knobs and assure stable calibration. It is powered by a light weight power supply (a kilohertz torroid core) which also supplies plus and minus 15 volts for the photo diode, FET, and operational amplifiers in the electronic sweep and sample circuits. Cord line dropping resistors are used to reduce the heat load in the box and increase the reliability of the transistors in the supply. A Motorola HEP bridge and large filter capacities supply a voltage that is regulated to about 75 volts. This voltage drives a DC-DC converter using high voltage HEP transistors (in parallel to provide current rating). The inverter is a high efficiency (special square loop tape-wound core) saturating square-wave oscillator. Multiple air-cooled secondary windings supply the voltage to full-wave bridges with a single output capacity. The 225 volts is derived from the 350 volts and regulated by Zener diodes.

The read-out circuits all use the identical integrated circuit chip (MC1433G) for simplicity of stocking spare parts. One chip forms a triangular (not a sawtooth) sweep. This is accomplished by feeding the integral of the snapping saturated square wave output into the inverting input and into the sweep output amplifier which supplies current, to charge the sampling capacitor (whose voltage is proportional

to the velocity and drives the output meter through an amplifier). The amplitude of the sweep (always the same dv/dt) and its mean position is controlled by the SPDT search-lock switch which changes the regenerative feedback by 5 and also feeds the meter output voltage into the circuit so that on "lock", the sweep circuit sweeps $\pm$ 10% about the signal. When a signal is received from the spectrum analyzer it is amplified and if large enough, triggers a threshold detector which charges up the sampling capacity to the voltage value of the sweep at that instant. A meter then reads the corresponding velocity. If the signal is lost, the voltage on the capacity will drift towards zero by the input current of the meter amplifier. (This capacitor can be recharged to full scale by pressing a reset button).

The required velocity reading range is 10 to 125 ft/sec. To accommodate this range and provide reading accuracy at lower velocity conditions, two scales are provided on the one meter; namely, 0 to 5[illegible] ft/sec and 0 to 150 ft/sec. The lower scale is provided by feeding only a third of the sweep voltage to the spectrum analyzer. Precision resistors provide the accurate negative offset to calibrate the low scale, and the constant impedance, 3:1 attenuator to match scales.

A second readout requirement is a measure of the velocity deviation (ΔV) about the mean value. A peak-to-peak voltmeter allows this information to be read on the velocity meter. In reality, two meters are provided on the velocimeter. One is located on the sensing head. The other is on the electronics cabinet. Values of ΔV (as well as mean velocity) are obtained from this remote meter depending upon a selector switch position.* Because of the finite number of fringes, a width to the frequency spectrum exists and so even a single velocity will show some ΔV.

* This meter reads 10 X ΔV.

2.5 VELOCIMETER TESTING

The portable sensing head and electronics cabinet which comprise the laser velocimeter are seen in the photographs of Figures 11 and 12, respectively.* Final testing was conducted with this apparatus at the conclusion of the program to verify basic operating characteristics. This was done qualitatively with flyash dust and water sprays, and quantitatively using water droplets and a spinning disc.

Calibration of the velocimeter was accomplished using a spinning disc in the following manner. An 18-inch diameter smooth white paper disc backed by 1/8-inch thick acrylic sheet, was installed on the shaft of an electric motor. The nominal motor speed was 1800 rpm.

The velocimeter was set-up before the disc with the optical axis approximately normal to the plane of the paper. The objective lens focus was adjusted until the two incident laser beams merged into a single spot. The distance between the target disc and entrance aperture on the instrument was measured and compared with the indicated objective lens range scale reading. The beam splitter was next adjusted to an equivalent reading. The distance (radius) from the motor shaft centerline to the center of the laser beam spot was measured before operating the motor.

Disc rotational velocity (shaft speed) was next measured using a Strobotac.** The velocimeter was allowed to sweep through the full frequency range until a signal "lock" was obtained at the lowest spectrum analyzer sensitivity setting. Velocity readings were made on both the high and low range meter scales. The remote (electronics cabinet) meter reading was compared with the sensing head meter. This procedure was repeated at different target distances to verify the accuracy of the range scale on the focusing objective lens.

---

* The operation and maintenance of this equipment is described in Reference 2.

** Product of General Radio Co., Cambridge, Massachusetts. Strobotac Type 631-VL, S/N 21705.

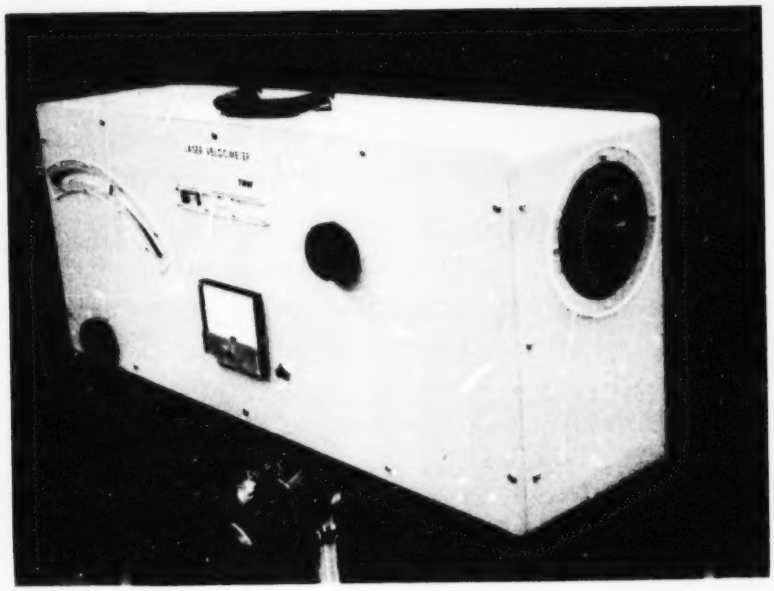

Figure 11. Laser velocimeter sensing head.

Figure 12. Velocimeter electronics package.

After these preliminary tests, the velocimeter was set up a distance of 10 feet from the target. A series of tests was made at different radii to check the velocimeter performance over the full velocity range. These data are plotted in Figure 13. An analysis of the data indicates a standard velocimeter measurement error of ±1.8 ft/sec over the range of 10 to 125 ft/sec. It is estimated that most of the velocity deviation can be attributed to small errors in reading the observed measurements. Some difficulty with the test setup was encountered in making measurements at the extreme high and low end of the velocity range. As a result, some apparent data scatter is seen at both ends of the curve in Figure 13.

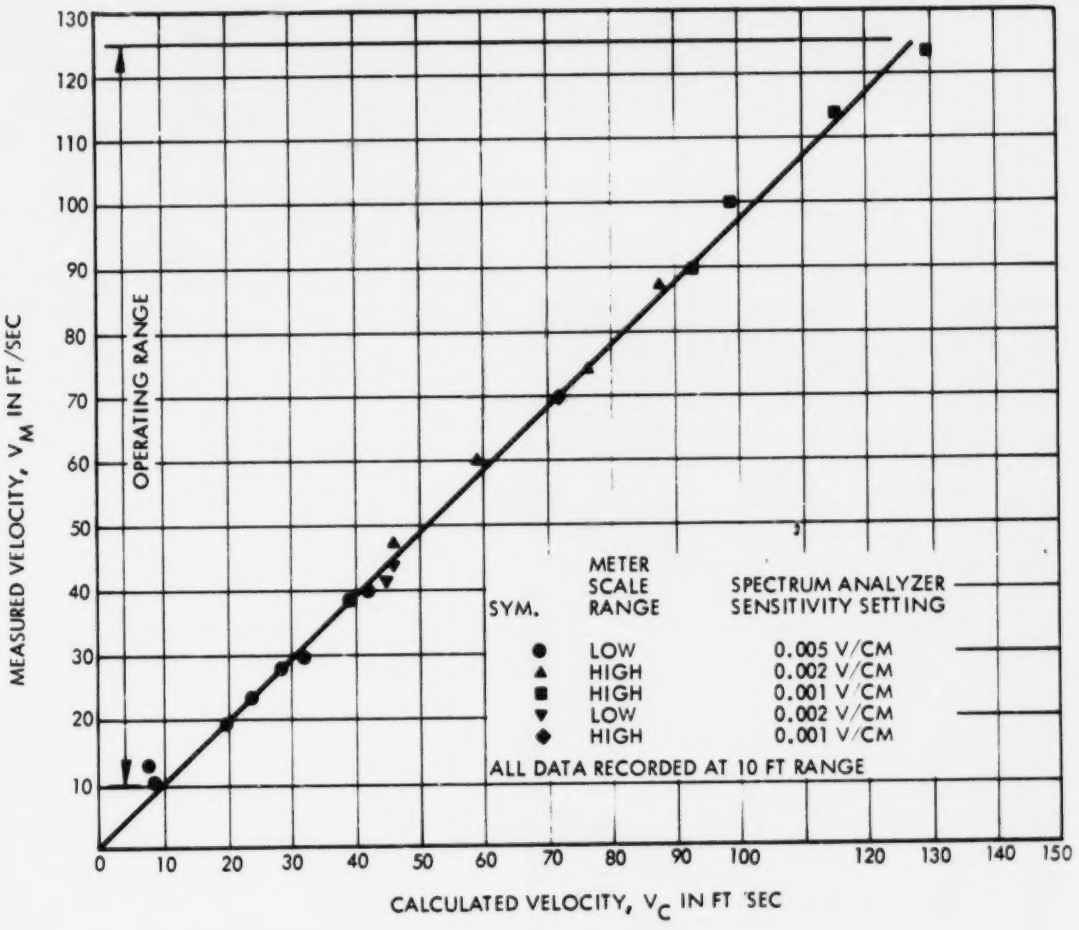
MEASURED VELOCITY, V_M IN FT/SEC
CALCULATED VELOCITY, V_C IN FT/SEC
OPERATING RANGE
METER SCALE RANGE
SPECTRUM ANALYZER SENSITIVITY SETTING
SYM.
LOW 0.005 V/CM
HIGH 0.002 V/CM
HIGH 0.001 V/CM
LOW 0.002 V/CM
HIGH 0.001 V/CM
ALL DATA RECORDED AT 10 FT RANGE
10 20 30 40 50 60 70 80 90 100 110 120 130
0 10 20 30 40 50 60 70 80 90 100 120 130 140 150

Figure 13. Plot of measured versus calculated velocity for laser velocimeter. Target was 18-inch-diameter spinning, white paper disc.

Additional laboratory tests were conducted using first flyash dust and later, atomized water sprays. The flyash tests were unsatisfactory in that the dust generator did not produce a uniform discharge. Rather, the particulate tended to clump together resulting in very heavy loadings resembling mostly dense clouds.

A commercial atomizing nozzle was substituted for the dust generator, with water droplets providing the scattering medium. The water spray proved more satisfactory in that the water flow rates could be varied by changes in feed pressure. Velocity measurements up to about 40 ft/sec were recorded by the velocimeter at ranges of 2 to 5 feet.

A velocimeter test was next made using a TRW low speed wind tunnel. The two-dimensional test section has a 5- x 24-inch cross section which then diverges linearly to an 8- x 24-inch cross section. Flow is directed vertically down through the 5-foot-long test section. Four turbulence damping screens and an aluminum honeycomb section are positioned just upstream of the tunnel's stagnation chamber. A tunnel contraction ratio of 8:1 further reduces turbulence intensities.

Both pitot tube and anemometer velocity measurements are used to measure test section velocities. The constant temperature anemometer is a TSI Model 1050 single tungsten wire probe. A TSI linearizer is used to provide analog output signals proportional to the velocity.

For the velocimeter test, the tunnel was operated at a constant speed core velocity of 58.7 ft/sec at the test section entrance. Air flow in the test section has a flat velocity distribution with a boundary layer velocity equal to 90 percent of the core velocity at a distance of 1/2 inch from the wall.

A water spray nozzle was installed at the entrance to the tunnel test section. Injection of a water spray into the tunnel air stream provided scattering centers for the laser velocimeter. These scatterers were intended to simulate flyash particles in a stationary power plant stack or duct.*

---

*Introduction of flyash or chemical aerosols into the closed-loop tunnel was rejected for reasons of tunnel contamination.

The nozzle was operated at a pressure drop (ΔP) of 30 lb/in^2 (limited by the available supply pressure). At this ΔP, the injection velocity V_j was calculated from the relationship $V_j = C_D[2g\Delta P/\rho]^{1/2}$, where: C_D is the orifice coefficient (assumed to be ~ 0.75); g is the gravitational constant equal to 32.174 ft/sec^2; and ρ is the density of water at 62.4 lb/ft^3. The injection velocity V_j was determined to be 50.06 ft/sec.

Water droplet velocities as a function of distance from the point of injection into the air stream were also estimated. A mean droplet diameter was calculated from the Ingebo correlation[3]. This empirical relationship yields a volume-number-mean droplet diameter D_{30} expressed by the following equation:

$$D_j/D_{30} = 2.64 \sqrt{D_j V_j} + 0.97\, D_j\, (V_{air} - V_j) \qquad (1)$$

where the water jet (orifice) diameter D_j and droplet diameter D_{30} have units in inches, and the air velocity V_{air} and water jet velocity V_j have units of ft/sec. In this instance, the injector orifice diameters were 0.040 inch and the wind tunnel air velocity was 58.7 ft/sec in the 5- x 24-inch cross section. From Equation (1) the mean droplet diameter was calculated to be 9.8×10^{-3} inch or approximately 250 microns.

Velocimeter droplet velocity measurements were made at axial distances of 2.3 and 4.6 feet downstream of the water spray injection point in the tunnel divergence section at a range of 6 feet. Average droplet velocities of 35 and 40 ft/sec were measured at the two locations. These measurements correspond to air velocities of 45.2 and 36.8 ft/sec, respectively. Velocimeter measurements at distances further downstream of the spray injection and at greater range were prohibited due to physical limitations of the wind tunnel test setup.

The apparent discrepancy between air velocity measurements and velocimeter droplet velocity measurements was subsequently analyzed. An expression was derived to estimate the average particle (droplet) velocity $\bar{V}_p$ as a function of distance X from the point of injection into the tunnel air stream. This derived relationship is

$$\bar{V}_{pf} = 1 - \left[\frac{D_{30}\,(1-\bar{V}_{pi})}{0.92\times10^{-3}\,C_D\,(X_f-X_i)(1-V_{pi}) + D_{30}} \right] \qquad (2)$$

where:

D_{30} = volume-number-mean droplet diameter

V_{pi} = initial droplet injection velocity

C_D = drag coefficient for a sphere based upon the local droplet and air velocities

and subscript f = final condition

i = initial condition

The results of this analysis are shown in Figure 14 where both air and estimated mean droplet diameter (D_{30}) velocities are plotted as a function of distance in the tunnel divergence section. Velocimeter measurements were within less than 5 percent of the predicted droplet velocities. In addition, droplet velocities did not achieve equilibrium with the test section core velocity.

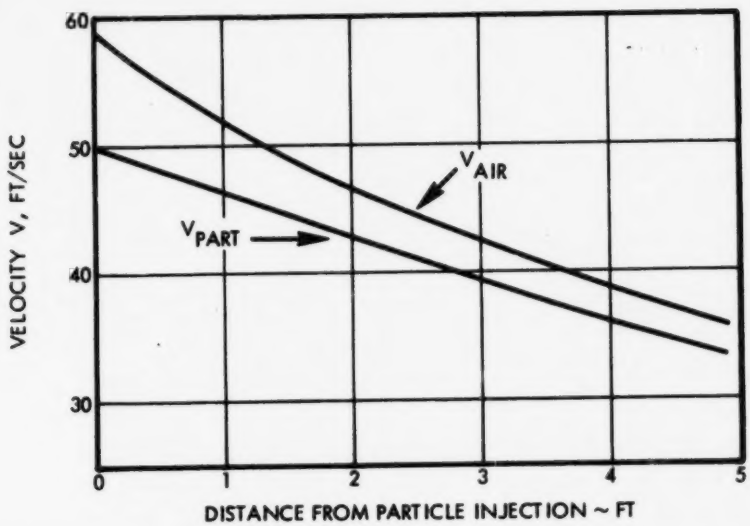

Figure 14. Air and predicted particle (droplet) velocity as a function of distance from particle injection into the divergent wind tunnel test section.

3. LONG RANGE OPTICAL VELOCITY METERS

3.1 INTRODUCTION

This discussion is concerned with the operation of optical velocity meters for use on large smokestacks, at ranges of 300 to 1500 feet (100 to 500 meters). The smoke velocity to be measured is assumed to be in the range of 10 to 125 feet per second (3 to 40 meters per second). The dust loading is in the range of 1 to 10 grains per standard cubic foot (2×10^{-6} to 2×10^{-5} grams per cm^3), and the mean particle diameters are assumed to have the values of 1μm, 10μm, or 50μm. As representative specific gravities of the particles, 0.5 gram per cm^3 or 1 gram per cm^3 is used.

Three types of optical velocity meters are considered here, all of which are single station instruments which rely on backscatter. The first type is called the direct doppler velocity meter. Its configuration is shown in Figure 15 where a single beam from a laser is

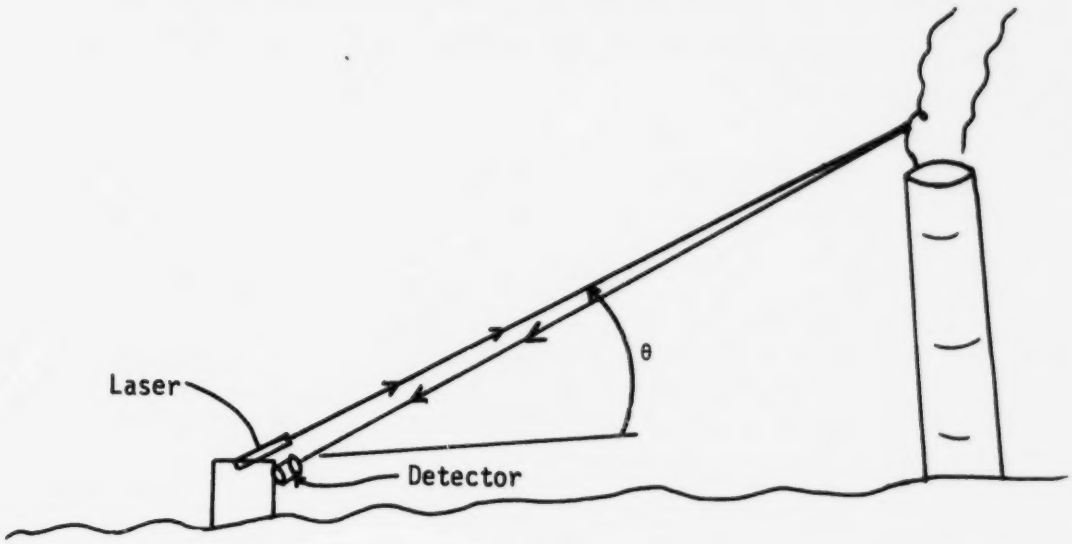

Figure 15. Direct doppler velocity meter.

pointed at the smoke, and the backscattered light is detected by a heterodyne detector, using a fraction of the laser's output as the local oscillator for detection. From the output frequency of the heterodyne detector, the smoke velocity can be obtained when the elevation angle θ is known.

The second type of velocity meter uses two beams from the same laser, which intersect each other at the region to be sampled (see Figure 16). In the intersection volume common to the two beams, a set of stationary interference fringes is formed. These fringes are effectively a set of "sheets of light." When an object passes through these fringes, the scattered light pulsates as the object passes from fringe to fringe. By measuring the pulsation frequency of the scattered light, one obtains the desired velocity information. This type of velocity meter is called the "fringe velocimeter."

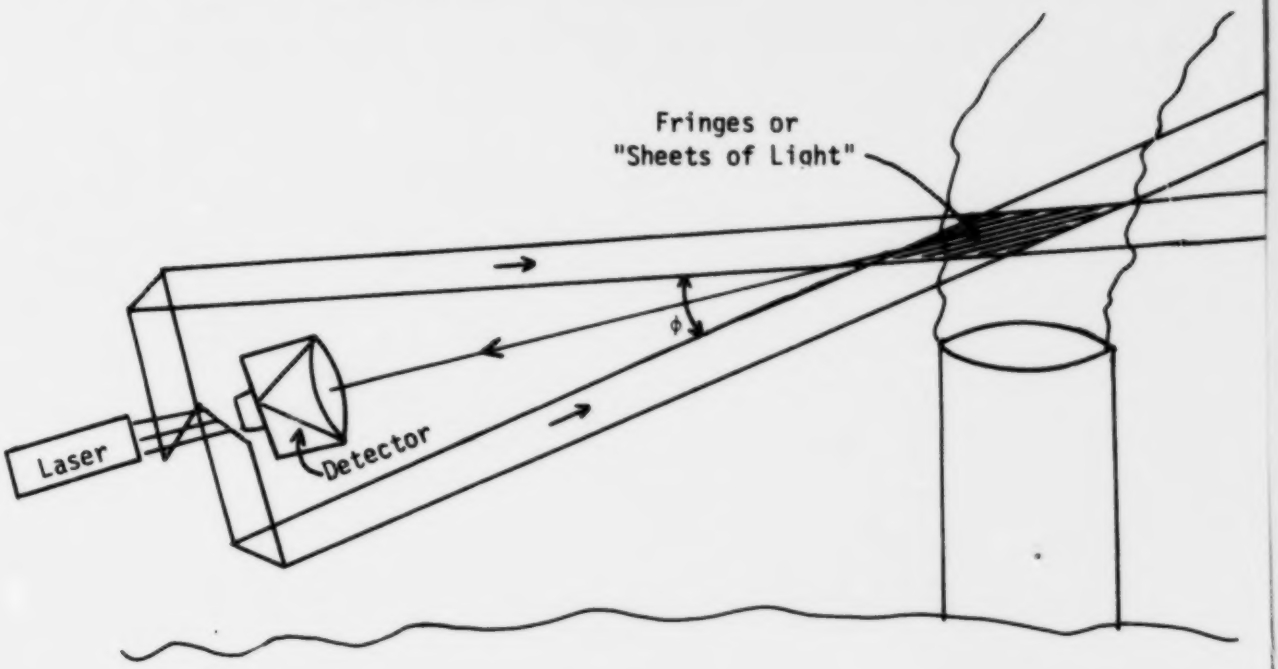

Figure 16. Schematic of fringe velocimeter.

This second instrument can also be explained purely in terms of doppler shifts from the two beams, and hence is also known as a form of laser doppler velocimeter. However, the fringe explanation is used because it makes many aspects of the operation more obvious and intuitive. The fringes can be observed directly if desired by placing a stationary card in the intersection region and examining the light on the card with sufficient magnification to reveal the fringes. Analytically, the two alternate explanations are equivalent.

The third type of velocity meter is called a "reticle velocimeter" and is sketched in Figure 17. This instrument is very simple and can use sunlight as its illumination source. It consists of a lens, like a telescope objective lens, which forms an image of the smoke on a reticle. The reticle pattern consists of black stripes on a transparent glass. Behind the glass is a photodetector. As a bright "blob" of smoke moves upward, its image passes over the reticle stripes and produces a pulsating output from the detector. The frequency of the pulsating

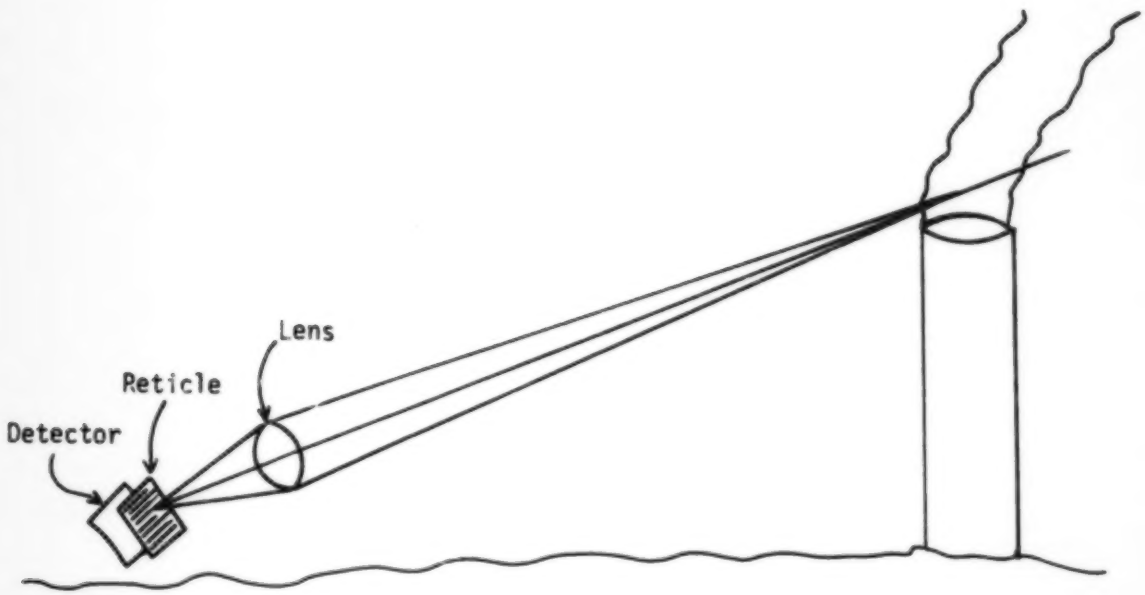

Figure 17. Reticle velocimeter.

detector output gives the velocity of the smoke. This instrument thus has considerable similarity to the fringe velocimeter. The reticle at the detector plays the same role that the fringes at the smoke play in the fringe velocimeter.

The remainder of this discussion will present information relevant to the performance of these three types of velocity meters under the smokestack conditions outlined at the beginning. Since all three of these meters present their velocity information as a somewhat periodic signal on a noise background, the system noise is an item of principal concern.

3.2 SMOKE OPTICAL PROPERTIES

For the performance evaluation, it is important to know the number of particles in the sampled volume. From the dust loading and particle data of the introduction, the number of particles per cubic centimeter may be computed. The results are shown in the following table.

Table I. Number of Particles per cm^3.

Particle Diameter	1 GRAIN/ft^3		10 GRAINS/ft^3	
	Specific Gravity = 1	Specific Gravity = 1/2	Specific Gravity = 1	Specific Gravity = 1/2
1 μm	4.5×10^6	9×10^6	4.5×10^7	9×10^7
10 μm	4.5×10^3	9×10^3	4.5×10^4	9×10^4
50 μm	3.7×10^1	7×10^1	3.7×10^2	7×10^2

A second characterization of the particle density is obtained by computing the mean free path of a photon in the smoke. For present purposes, it is sufficient to use the geometric cross section rather

than the more refined true optical cross section. Thus, the mean free path is given by $\frac{1}{n\sigma}$, where n is the particle density and σ is the geometrical cross section area of the particle. The mean free path results are shown in Table II.

Table II. Mean Free Path of Light in Smokes

Particle Diameter	1 GRAIN/ft^3		10 GRAINS/ft^3	
	Specific Gravity = 1	Specific Gravity = 1/2	Specific Gravity = 1	Specific Gravity = 1/2
1 μm	28 cm	14 cm	2.8 cm	1.4 cm
10 μm	280 cm	140 cm	28 cm	14 cm
50 μm	1400 cm	700 cm	140 cm	70 cm

3.3 SAMPLE VOLUME SIZE

Before conclusions can be drawn from the foregoing tabular data, it is necessary to know the volume and shape of the region sampled. For the first two instruments, this volume consists of the intersection of two beams (or of one beam and one observing path). The configuration is shown in Figure 18.

For a lens of diameter d, the minimum possible width of the beam at range r is given approximately by

$$w = \lambda \frac{r}{d} \quad ,$$

where λ is the wavelength of light. For a 4-inch (10 cm) lens at 100 meters range, this gives w = 1/2 mm, and at 500 meters w = 2.5 mm. These values are based on diffraction-limited performance, and in view of the turbulent air encountered in the intended operation, it would appear unwise to base an instrument on this high a performance standard. This standard of performance corresponds to a telescope of about 100 power or greater. The military seldom uses telescopes of powers greater than 20 because too often the turbulence renders higher powers useless. Thus,

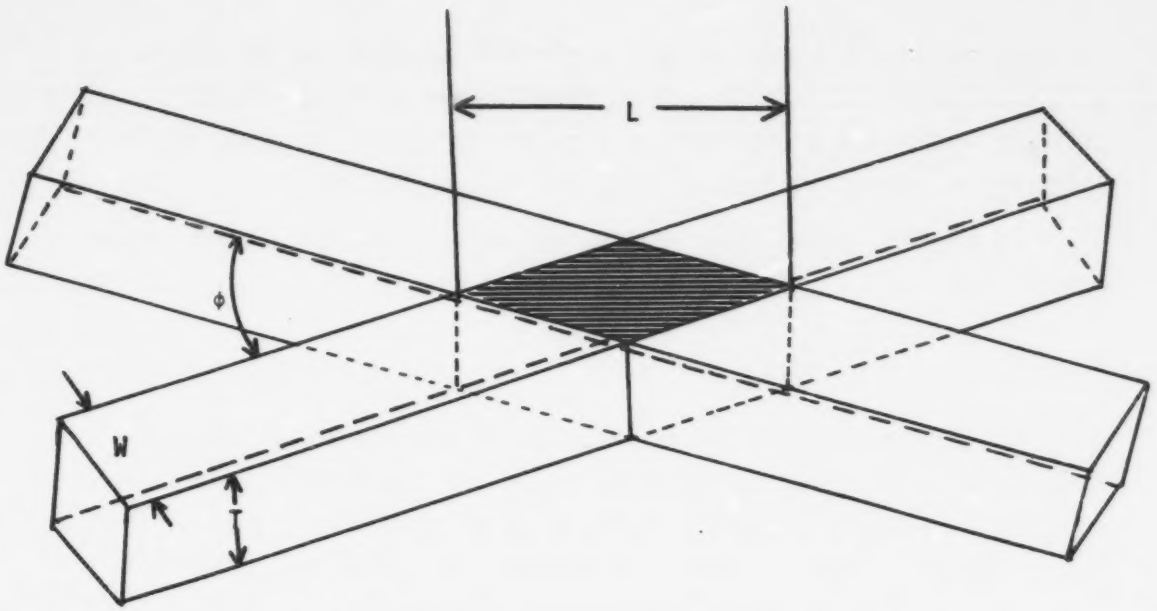

Close-up of Intersection Volume

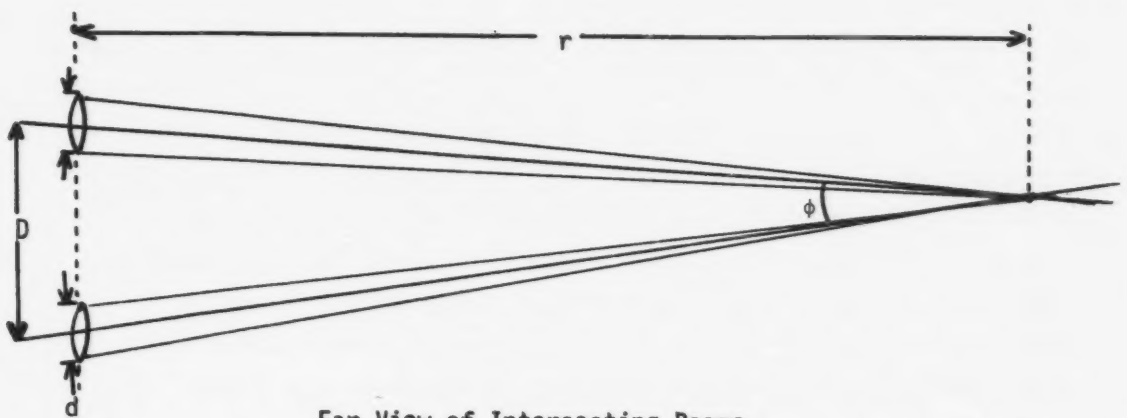

Far View of Intersecting Beams

Figure 18. Beam intersection geometry.

it seems prudent to expect at most a 2.5 mm beam width at 100 meters and a 12.5 mm beam width at 500 meters, these values being 1/5 of the diffraction-limited performance of a 4-inch objective, or equal to the diffraction-limited performance of a 0.8-inch objective.

The length L of the intersection volume is given (to a close approximation) by

$$L = 2w \frac{r}{D} \quad ,$$

where D is the separation of the two beams at the observing station. Since very high precision alignment between the two beams is required for convenient operation, the beam optics must be mounted on a common rigid unit. For a 2-meter separation, about the maximum that seems practical, this gives an L of 0.25 meter at 100 meters range, and 1.25 meters at 500 meters range. An instrument with such a large separation would require a special truck. Moreover, the large separation allows turbulence to affect the beams independently, which introduces extra noise into the system.

Referring to Table II, where the mean free path is given, it is clear that for the small particle or heavy loading conditions, severe attenuation of the beam both on its inward pass and on its outward pass will contribute to the difficulty of obtaining range resolution. Moreover, multiple scattering also imposes additional difficulty in obtaining range information by degrading the signal-to-noise ratio when probing several mean free paths deep. Because of these difficulties, it appears appropriate to concentrate attention first upon a more convenient instrument which makes no attempt to obtain range information, but simply probes the plume with a long thin sample volume. The returning information will then be primarily from the region of the near side with a depth approximately one-half of the mean free path. Unless otherwise stated, the remainder of the discussion is limited to instruments with long thin probe volumes having no range resolution. At a later time, it may be appropriate to consider more sophisticated instruments with range resolution.

3.4 SIGNIFICANCE OF THE SMOKE OPTICAL PROPERTIES IN CONJUNCTION WITH THE SAMPLE VOLUME SIZE

Three points of importance need emphasis. The first is that the number of particles in the sample volume is large. Even with the smallest beam width of 2.5 mm and the lightest loading of coarse particles, there would still be about 600 particles in the sample volume across a 3 meter diameter stack. For all other conditions, the number of particles in the probe volume is much greater.

The second point to note is that the mean free paths are generally much shorter than the length of the probe volume and of the stack diameter. Under these conditions, the amount of power backscattered can most easily be handled by a simple reflectivity coefficient rather than dealing with the scattering functions from individual particles. Caution must be exercised with white smokes where multiple scattering may cause complications, to be noted later. Under these short mean free path conditions, a change in smoke density does not change the amount of reflected light. This absence of density dependence is most disadvantageous for the fringe velocimeter. In the fringe velocimeter, it is desired that as a density fluctuation, say a small local increase in density, passes by the fringes, a pulsating return signal is produced. However, in the case where the mean free path is short compared to the probe volume, no pulsation of the return is obtained because the density variations simply allow the light to penetrate a little more or less so that the same number of particles are always involved, resulting in a constant return. This phenomenon is referred to as "contrast washout."

A third point to note is that the mean free paths are longer than the scale of some of the turbulent eddies. This results in a spread of velocity components along the viewing direction. As will be explained later, this spread creates a "granularity" noise which is significant in the laser-illuminated cases.

3.5 SHOT NOISE OF DETECTION

One of the principal sources of noise in the instruments under consideration is the shot noise of the detection process. This noise arises from random fluctuations in the emission times of the electrons at the photocathode of the detector. In systems using photomultipliers, this source of noise is often dominant over other sources, such as thermal agitation noise.

To develop a formula for the signal-to-noise ratio due to shot noise, the incoming light flux is represented in the form

$$S(t) = S_0 + S_1(t) + S_2(t) \quad .$$

Here, $S(t)$ represents the light power (in watts) falling upon the detector and as indicated in the above formula, this is represented as the sum of three terms. The first term S_0 is the average dc power of the light. The second term $S_1(t)$ represents those fluctuation components within the signal pass band of the instrument; that is, $S_1(t)$ is the desired signal. The third term, $S_2(t)$ represents those fluctuation components outside the signal pass band. The average values of $S_1(t)$ and $S_2(t)$ are zero, since S_0 is the dc average of $S(t)$.

The photocathode current is then given by

$$i(t) = \eta e \frac{1}{h\nu} [S_0 + S_1(t) + S_2(t)] \quad ,$$

where η is the quantum efficiency of the photodetector (electrons per photon), e is the electronic charge, h is Planck's constant, and ν is the optical frequency. After this current is passed through the band pass filter, there remains the signal,

$$i_{sig}(t) = \eta e \frac{1}{h\nu} S_1(t) \quad .$$

When this current is passed through a resistor, R, the time-averaged signal power is then

$$i_{sig}^2 R = \eta^2 e^2 \frac{R}{(h\nu)^2} \overline{S_1}^2 \quad , \tag{3}$$

where

$$\overline{S_1}^2 = \lim_{T\to\infty} \frac{1}{T} \int_0^T S_1^2(t)\, dt \quad .$$

The shot noise power in the pass band is given by

$$2eIR\Delta f \quad ,$$

where e is again the electronic charge, R is the same load resistor, and Δf is the bandwidth of the pass band.* Here I is the average photocurrent and hence is given by

$$I = \eta e \frac{1}{h\nu} S_0 \quad .$$

Combining these, the shot noise power in the pass band is given by

$$2e^2 \eta \frac{1}{h\nu} R S_0 \Delta f \quad . \tag{4}$$

Taking the quotient of (3) and (4), gives the signal-to-noise ratio,

$$\frac{\text{Signal Power}}{\text{Shot Noise Power}} = \frac{1}{2\eta} \frac{1}{h\nu} \frac{\overline{S_1}^2}{S_0 \Delta f} \quad . \tag{5}$$

This formula can be written in a form so as to have an easily visualized content. To do this, note that

$$\eta \frac{1}{h\nu} S_0 \frac{1}{\Delta f} \tag{5.5}$$

is the average number of detected photons (i.e., photoelectrons) in the time interval $\frac{1}{\Delta f}$. The time interval $\frac{1}{\Delta f}$ corresponds to the time of one full cycle at a frequency corresponding to the bandwidth. Thus, one can write

---

* American Institute of Physics Handbook, Section 6m, "Radiation Detection."

$$\frac{\text{Signal Power}}{\text{Shot Noise Power}} = \frac{1}{2}\left(\begin{array}{l}\text{Average number of}\\ \text{detected photons}\\ \text{in time interval } \frac{1}{\Delta f}\end{array}\right) \cdot \frac{\overline{S}_1^2}{S_o^2} \quad . \qquad (6)$$

The fraction $\overline{S}_1/S_o$ can be thought of as the modulation index or modulation depth of the incoming light. It is the ratio of the RMS signal component to the average light power.

Note that it is the number of <u>detected</u> photons which enters the signal-to-noise ratio formula. Thus high quantum efficiencies are desirable, as well as high powers of the light itself. Also, narrow bandwidths favor the signal-to-noise ratio, for they provide longer time intervals $\frac{1}{\Delta f}$ for the detection of photons in (6).

Formula (6) can be used to determine the required laser power output to achieve a given signal-to-noise ratio. However, the pass band Δf and the modulation depth for each system must first be determined.

3.6 THE DIRECT DOPPLER SYSTEM

In order to maximize the signal-to-noise ratio, it is desirable to keep the pass band as small as possible without losing signal. The signal width for the direct doppler instrument is determined by turbulence within the smoke. Referring to the following sketch (Figure 19), the observing line

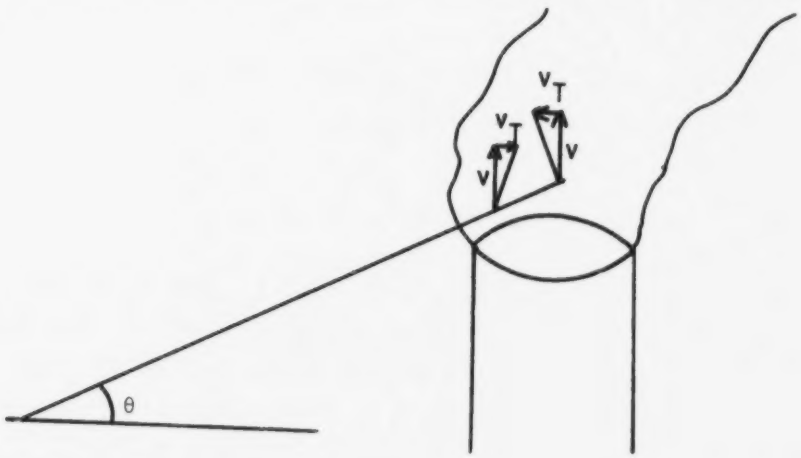

Figure 19. Effect of turbulence on direct doppler system.

is at an elevation angle θ. Within the sample volume, the average vertical component of velocity is denoted by v. This is the velocity which it is desired to measure. Because of the turbulence, there is added to v a turbulent velocity, v_T. As a rough guide, the turbulent velocities can be taken to be about 10 percent of the main flow velocity v. These turbulent velocities can be in any direction, and thus some will be along the sight line.

The component of the main flow velocity along the sight line is $v \sin \theta$. Thus, the average doppler frequency is

$$f_{ave} = \frac{v}{\lambda} \sin \theta \quad . \tag{7}$$

When a turbulent velocity v_T occurs along the line of sight, the frequency will be

$$f = \frac{1}{\lambda}(v \sin \theta \pm v_T) \quad .$$

Thus, the spread in frequency due to turbulence is

$$\Delta f = 2 \frac{v_T}{\lambda} \quad . \tag{8}$$

Combining (8) with (7), one obtains

$$\frac{\Delta f}{f} = 2 \frac{v_T}{v} \frac{1}{\sin \theta} \quad . \tag{9}$$

This equation exposes an important limitation of the direct doppler velocimeter as applied to the present turbulent smokestack case; namely, if the elevation angle θ is too small, then the turbulence causes a spread in the signal frequency comparable to the basic doppler frequency itself. Under these conditions, it is impractical to obtain the desired velocity information.

At steep elevation angles, some determination is possible. For example, at 45 degreees with the value of $v_T/v = 1/10$ (turbulent velocities 10 percent of main flow), then $\Delta f/f = 0.28$. With such an instrument, a 10% determination of average velocity may be possible.

The preceding limitation may possibly be overcome with highly sophisticated systems which "track" the turbulent velocity fluctuations, thus permitting an effective narrow pass band and accurate determination. The investigation of such a sophisticated system is beyond the scope of the present report. In this connection, note that due to the fact that the depth of penetration is larger than some turbulence cell diameters, the returning signal is not a single frequency shifting about, but a complex composite with different frequency components simultaneously present from the different parts of the sample volume moving at different velocities.

For the direct doppler instrument, the best signal-to-noise ratio is obtained with a reference that is strong compared to the signal. Under this condition, formula (6) becomes

$$\frac{\text{Signal Power}}{\text{Noise Power}} = \left(\begin{array}{l} \text{Average number of detected} \\ \underline{\text{signal}} \text{ photons in the} \\ \text{time interval } \frac{1}{\Delta f} \end{array} \right) . \qquad (10)$$

(This formula assumes that the reference source does not contain any excess noise, a matter of practical concern.)

This formula can be applied to predict the required laser power output for a direct doppler instrument. Example conditions are as follows:

Elevation Angle θ	= 45 degrees
Slant Range	= 100 meters
Reflectivity of Smoke	= .1
Receiving Aperture	= .01 m^2 (4.5 in. diam. lens)
Quantum Efficiency	= .1
Wavelength	= .5 μm
Smoke Velocity	= 40 meters/second
Turbulent Velocity/Flow Velocity	= .1
Signal-to-Shot Noise Ratio	= 10

These conditions, together with the foregoing formulas, yield the following:

Center Frequency	57 MHz
Bandwidth	16 MHz
Required Laser Power	.02 watt

It thus appears that a direct doppler instrument may be a possibility inasmuch as argon lasers with considerably greater power than the above are available.

However, there are many further considerations beyond the fundamental one of shot noise. There are additional sources of noise, for example, thermal agitation noise, noise associated with the photomultiplier multiplication process, and noise from fluctuations of the laser intensity and intermode beating. Background light which is inadequately filtered out is an additional source of noise. Moreover, operation of a photomultiplier at a frequency of 57 MHz requires proper design. For the direct doppler system to work as described above, it is required that the illuminated spot on the smoke supplied by the laser be at least as small as the theoretical resolution limit of the receiving lens. In addition, turbulence along the path can spoil the resolution, which in turn can decrease the signal-to-noise ratio. Multiple scattering in the smoke can also increase the size of the illuminated spot from which the light returns, and this too degrades the signal-to-noise ratio.

The coherent detection process used in the direct doppler type instrument only functions as described above with light from particles within the theoretical limit focal volume. This is a cylindrical volume approximately $\lambda \frac{r}{d}$ in diameter and $\lambda (r/D)^2$ in length. For the above example, this is a cylinder 0.5 mm in diameter by 0.5 meter long. Light returning from particles outside this volume does not have a uniform phase relationship with the reference light over the full entrance aperture. The result is that light from particles outside this cylindrical volume contributes little or nothing to the signal. Such light can increase the noise level, however. This requirement of a uniphase wavefront is a fundamental limit imposed by the coherent detection process. The uniphase condition can be achieved more easily with smaller receiving apertures, but they collect less light which strains the system in another direction.

Still another demand of the direct doppler system is that either the laser must have a coherence length equal to the round trip to the sample volume and back, or that an optical delay be provided for the reference light equal to the round trip distance. This is necessary to insure that the reference be coherent with the returning signal.

In summary, the direct doppler type instrument appears to have the following properties: Nearly horizontal paths cannot be used due to the turbulence contribution. Elevation angles on the order of 45 degrees appear necessary, and these eliminate long range applications. A one-watt or greater argon laser is required to give a comfortable signal-to-noise ratio. Careful attention must be paid to many noise sources and to the high frequency detector design. The velocity measurement is not likely to be better than 10 percent, and will have no depth resolution.

3.7 THE FRINGE VELOCIMETER: GRANULARITY NOISE

Before turning to an evaluation of the fringe velocimeter, it is appropriate to discuss a source of noise relevant to the fringe velocimeter. This source is called granularity noise because of its relation to the granularity or speckle pattern produced when a laser illuminates a diffuse surface. The origin of this noise is shown in the following sketch (Figure 20):

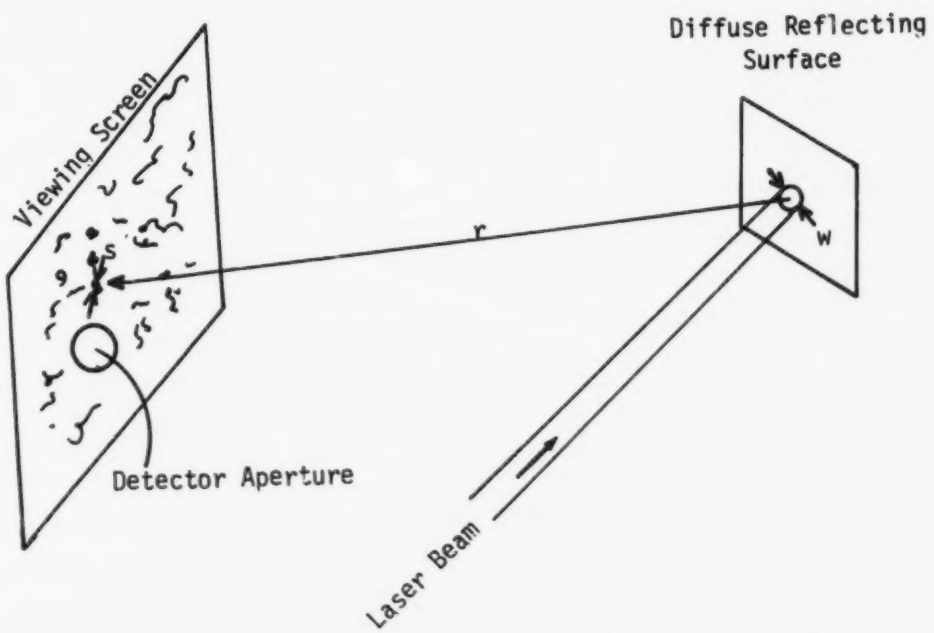

Figure 20. Granularity noise in the fringe velocimeter.

In this sketch, a laser beam is shown illuminating a spot of diameter w on a diffuse reflecting surface. The light reflected from this surface travels in all directions, and at range r there is placed a large white viewing screen. It will be found that the light intensity on the viewing screen is not uniform, but has a speckled or granular appearance. This stems from the monochromatic nature of the laser.

The intensity at a given point of the viewing screen is found by adding up the amplitudes from all the different points composing the illuminated spot of diameter w. This is a phase addition with the phases randomized by the diffuse nature of the reflecting surface. At some points, the phases will largely cancel each other, resulting in a low intensity or dark spot. At other points, the phases will be largely in phase, resulting in a bright spot.

The "size", s, of these granules, on the viewing screen, is approximately given by

$$s = \lambda \frac{r}{w} \quad . \tag{10.5}$$

Actually, the distribution is random, and what is meant by the above is that two points closer together than s will not have independent intensities, but will be correlated. To the eye, the characteristic apparent "diameter" of the granules is given by s.

[In the direct doppler instrument, the uniphase wavefront requirement discussed earlier corresponds to the condition that the receiving aperture be no larger than the size of one granule, i.e., be of diameter $\leq$ s.]

In the present smokestack application, the motion of the smoke causes the granularity pattern to change in time, which creates intensity fluctuations at the detector. These constitute noise, and it is necessary to evaluate the amount of this noise which is in the pass band of the instrument.

It can be shown that the RMS fluctuation in light power entering detector, ΔP, is given by

$$\Delta P = P_a \frac{1}{\sqrt{M}} \quad , \tag{11}$$

where P_a is the average light power entering the detector and M is the number of granules present in the detector aperture. (The foregoing assumes that the returning light is still polarized after reflection. If not, M should be replaced by 2M in Equation 11.) If the detector aperture diameter is D, then

$$M = \left(\frac{D}{s}\right)^2 \quad . \tag{12}$$

Notice that if M = 1 corresponding to $D = s$, then the RMS fluctuation is equal to the average light power. By making the receiver aperture large so that M becomes large, or by making w large so that s becomes small and hence M large. these granularity fluctuations are reduced, decreasing the system noise.

To evaluate the significance of this granularity noise, we need to determine how rapidly the pattern changes, and what fraction of the noise is in the instrument's pass band.

If the smoke were a rigid mass moving uniformly upward, then when the smoke has moved upward a distance w, all new particles would be in the illuminated region, and a new granularity pattern would be present. Thus, the upper frequency limit of the granularity noise is given by

$$f_{\substack{\text{max} \\ \text{rigid smoke}}} = \frac{v}{w} \quad , \tag{13}$$

where v is the smoke velocity.

However, rigid translation of the smoke upwards is not the only source of change in the speckle pattern. Recall that in the present application, the probe volume length is long enough to span more than one turbulent cell. Thus, the reflector is effectively a set of two or more partial reflectors which are in motion relative to each other. When the relative motion is of the order of one wavelength, then the phase addition is uncorrelated with the previous addition, and a new speckle pattern is formed. Thus, letting v_T denote the turbulent velocity components as

before, and recognizing that some of these occur along the line of sight, the apparent frequency of speckle pattern change due to turbulence is approximately given by

$$f_{max} = \frac{v_T}{\lambda} \quad . \tag{14}$$

Inasmuch as v_T is approximately 1/10 of v, the frequency given by (14) is much higher than that given by (13), for realistic values of w in the present application. Thus, formula (14) is the proper one to use for estimating the effects of granularity noise in the realistic case.

By comparison with other aspects of speckle behavior, it is inferred that the frequency (power) spectrum of this noise is, to an accuracy sufficient for present purposes, approximately flat from zero up to f_{max}, given by (14). On this basis, the RMS fluctuation of the arriving light due to granularity noise in a pass band of width Δf may be found by combining (11) and (14).* The result is

$$\text{(RMS Granularity Fluctuation of Arriving Light)} = P_a \frac{1}{\sqrt{M}} \sqrt{\frac{\Delta f}{f_{max}}} \quad ; \tag{14.5}$$

hence,

$$\text{(RMS Granularity Fluctuation of Arriving Light)} = P_a \frac{1}{\sqrt{M}} \sqrt{\frac{\lambda}{v_T} \Delta f} \quad . \tag{15}$$

---

* To obtain the portion in the pass band, it is necessary to use the fluctuation power (the square of the RMS). The fraction $\Delta f/f$ of this total fluctuation power is within the passband. The square root of this fraction gives the RMS of the fluctuations in the pass band. An alternate argument leading to the same result is that the basic fluctuations occur every $1/f_{max}$ seconds. The number of basic fluctuations in the time interval $1/\Delta f$ is therefore $f_{max}/\Delta f$. The RMS value of the sum of $f_{max}/\Delta f$ samples is $\sqrt{\Delta f/f_{max}}$ times the RMS of the basic fluctuation RMS given by (11), which yields the formula (14.5).

To obtain a signal-to-noise ratio, it is necessary to consider the signal and the pass band Δf over which the signal is spread. For the fringe velocimeter, let Λ denote the spacing of the fringes and N denote the total number of fringes across the probe volume's width W. Then:

$$N\Lambda = W \quad . \tag{16}$$

The output frequency due to particles crossing the fringes with velocity v is

$$f_{signal} = \frac{v}{\Lambda} \quad . \tag{17}$$

Since there are N fringes across the probe volume, it can be shown that the spectral width Δf_{signal} of the signal is given approximately by

$$\Delta f_{signal} = f_{signal} \cdot \frac{1}{N} \quad . \tag{18}$$

Combining (15) with (16), (17), and (18) yields the granularity noise in a pass band which just passes the signal. The result, after appropriate cancellation, is

$$\left(\begin{array}{c}\text{RMS Granularity Fluctuations of Arriving} \\ \text{Light in Signal Pass Band}\end{array}\right) = P_a \frac{1}{\sqrt{M}} \sqrt{\frac{\Lambda}{W} \frac{v}{v_T}} \quad . \tag{19}$$

Attention is next turned to the signal. If one particle at a time passes through the intersection volume, the returning light is 100 percent modulated by the fringes. However, as more particles are simultaneously present in the probe volume, the returning light is less modulated because some particles are "on" the fringes at the same time that others are "off" the fringes. It can be shown that if the particles are randomly distributed, the following relation holds:

$$\left(\begin{array}{c}\text{RMS Fluctuation of Arriving} \\ \text{Light Power Due to Signal}\end{array}\right) = \frac{1}{\sqrt{2}} P_a \frac{1}{\sqrt{m}} \quad . \tag{19.5}$$

where P_a is again the average light power returned to the detector, and m is the total number of particles returning light from the probe volume. This signal is spread over the frequency interval Δf_{signal} given by (18).

Dividing this by (19) yields the following ratio,

$$\left(\frac{\text{RMS Signal Fluctuation}}{\text{RMS Granularity Fluctuation}}\right) = \sqrt{\frac{1}{2}\,\frac{w}{\lambda}\,\frac{v_T}{v}\,\frac{M}{m}} \quad . \qquad (20)$$

The ratio (20) is the ratio between the RMS fluctuation of the arriving light flux due to the signal, and the RMS fluctuation of the light, due to granularity, each within the signal passband. After detection, these light fluctuations become fluctuations in a current (or voltage). Since the power in the signal or noise is proportional to the square of the current (or voltage), the signal power to granularity noise power ratio is the square of the ratio given in (20), namely,

$$\frac{\text{AC Signal Power}}{\text{Granularity Noise Power}} = \frac{1}{2}\,\frac{w}{\lambda}\,\frac{v_T}{v}\,\frac{M}{m} \quad . \qquad (21)$$

This may be evaluated with the aid of the particle densities given earlier in this report.

The special case in which the mean free path is short compared to the stack diameter yields a particularly informative relation. For this case, the total number, m, of particles returning light is approximately

$$m = \frac{1}{2}\, n\, w^2 \left(\frac{1}{\sigma n}\right) \quad ,$$

since $\frac{1}{\sigma n}$ is the mean free path, n being the particle density. Moreover, to first approximation $\sigma \simeq \delta^2$, where δ is the particle diameter. Substituting these in (21) yields

(Case of short mean free path)
$$\frac{\text{AC Signal Power}}{\text{Granularity Noise Power}} = \frac{\delta^2}{\lambda w}\,\frac{v_T}{v}\,M \quad .$$

Using (10.5) and (12), this relation may be written,

$$\frac{\text{AC Signal Power}}{\text{Granularity Noise Power}} = \left(\frac{\delta}{\lambda}\right)^2 \frac{v_T}{v} \left(\frac{D}{r}\right)^2 \frac{w}{\lambda} \quad . \qquad (22)$$

The factors δ/λ and v_T/v are properties of the smoke, and thus for operation at a given range, the designer has only the lens diameter D and the probe volume width w with which to secure a favorable signal to granularity noise ratio. The formula indicates that large values of both D and w are desirable. It will be seen later that for random particle distribution, a small value of w is desired to enhance the signal-to-shot noise ratio. Thus, an optimum w exists which minimizes the sum of granularity and shot noise powers.

It should be noted that the uniformly random distribution yielding formula (19.5), on which the above is based, may not give a true description of the behavior. It seems reasonable that local clumping due to turbulent eddies may occur, and if these clumps are comparable in size to the fringes, the clumps may serve as large "particles", giving rise to much better performance than given by (21) and (22). On the other hand, for the short mean free path case, there can be a contrast washout because a region of low particle density simply lets the beam penetrate further until the backscatter is the same as for a higher density region. In this case, the true situation can be worse than predicted by (21) and (22).

Notice that the ac signal power-to-granularity noise power is independent of the laser power. Thus, one must arrange the system so that this ratio has a favorable value, and then use the formula for signal-to-shot noise ratio given much earlier (formula 6) to determine the required laser power.

3.8 FRINGE VELOCIMETER: REQUIRED LASER POWER

As an illustration, formula (6) or (5) is next applied to a representative case to estimate the required laser power. Again assuming a random particle distribution in the sample volume, it follows

that the modulation depth $\bar{S}_1/S_o$ of the received light has the value $\frac{1}{\sqrt{m}}$ where m is again the number of particles in the sample volume. Thus, the factor $\bar{S}_1^2/S_o^2$ in (6) has the value 1/m .

The time interval $\frac{1}{\Delta f}$ is determined by the signal bandwidth, and is given by $\frac{w}{v}$, where v is the smoke velocity to be measured, and w is the probe volume's width. This follows from formulas (16), (17), and (18).

Substituting these values in formula (6), and incorporating appropriate geometric factors for the fraction of laser light collected, the following is obtained:

$$\frac{\text{Signal Power}}{\text{Shot Noise Power}} = \frac{1}{2}\left(\eta\rho\, P_L \frac{A}{\pi r^2}\frac{1}{h\nu}\frac{w}{v}\right)\frac{1}{m} \quad , \qquad (23)$$

where

η = quantum efficiency of the detector
ρ = reflectivity of the smoke
P_L = laser power output
A = area of the detector collection aperture
r = range
$h\nu$ = energy of a photon (4×10^{-19} joules for 0.5 μm light).

The quantity in parentheses is the average number of photons detected in time interval $\frac{1}{\Delta f}$.

Denoting the probe volume's length by L:

$$m = n\, w^2 L \quad , \qquad (24)$$

where n is the particle density.

Incorporating this into formula (23):

$$\frac{\text{Signal Power}}{\text{Shot Noise Power}} = \frac{1}{2}\,\eta\rho\, P_L \frac{A}{\pi r^2}\frac{1}{h\nu}\frac{1}{v}\,\frac{1}{nwL} \quad . \qquad (25)$$

If it is further assumed that the mean free path, $\frac{1}{n\sigma}$, is short compared to the stack diameter, and that the particle cross section σ is approximately δ^2, where δ is the particle diameter, then:

(Short mean free path case)

$$\frac{\text{Signal Power}}{\text{Shot Noise Power}} = \frac{1}{2}\,\eta\rho\,P_L\,\frac{A}{\pi r^2}\,\frac{1}{h\upsilon}\,\frac{1}{v}\,\frac{\delta^2}{w} \quad . \qquad (26)$$

Notice that both formulas (25) and (26) show that small values of w are desirable in order to improve the signal-to-noise ratio. This stems basically from the fact that small values of w correspond to fewer particles in the probe volume, which makes the fluctuations proportionately greater. As noted earlier, this is based upon a completely random particle distribution, and may not apply if turbulence causes local clumping.

If the particle distribution is truly random, then the small values of w required by (25) and (26) prevent using large values of w to combat the granularity noise. In this event, a large receiving aperture is the only method for providing a large M to combat granularity noise.

An example of the power required by formula (26) is given below. The example conditions are similar to those of the direct doppler example; however, the receiving aperture is increased to keep the granularity noise down.

Conditions:

Range r	= 100 meters
Reflectivity of Smoke ρ	= .1
Receiving Aperture A	= .04 m^2 (9 in. diam. lens)
Quantum Efficiency η	= .1
Wavelength	= .5 μm
Smoke Velocity v	= 40 meters/second
Signal-to-Shot Noise Ratio	= 10
Particle Diameter δ	= 10 μm
Probe Volume Width w	= 25 mm
Turbulent Velocity/Flow Velocity	= .1

These values yield the following:

Required Laser Power	= .05 watt

The foregoing does not depend on the number N of frinues across the probe volume because it is assumed that the optimum bandwidth is used. However, to give a feeling of the frequencies involved, it is further assumed that N = 10, in which case:

Signal Frequency = 16 kHz
Signal Frequency Width = 1.6 kHz

In conjunction with formula (20), the example conditions yield

$$\frac{\text{Signal Power}}{\text{Granularity Noise Power}} = 8 \quad .$$

The example conditions are for the near range conditions of 100 meters. For the far range conditions of 500 meters, the situation is more demanding. In formulas (22), (25), and (26) one observes an r^2 dependence. In addition, w may depend on r, depending on the optical configuration.

It is to be emphasized that the example conditions are given as a guide to scale from, not as a design. In particular, the smoke reflectivity may be quite different, and a signal-to-noise ratio of 10 is not a comfortable design point in view of other secondary noise sources.

3.9 RETICLE VELOCIMETER NOISE ESTIMATE

A performance estimate for the reticle velocimeter is not easy to make because of unknown smoke properties.

It appears desirable to sample the flow immediately after it emerges from the stack, for otherwise large vortices of entrained air will complicate the situation and reduce the accuracy.

The contrast of the issuing smoke is not known. When sunlight is used as the light source, its direction is automatically different from the viewing direction, and hence the contrast washout mentioned earlier does not apply. It seems likely that performance can be optimized by choosing a viewing direction appropriately oriented relative to the sun.

As with the fringe velocimeter, the relative signal bandwidth $\frac{\Delta f}{f}$ is given to first approximation as $\frac{1}{N}$, where N in this case is the number of reticle lines across the field of view. This first approximation will be correct if the smoke "blobs" remain intact long enough to traverse the field of view. If not, the spectrum will be broadened. Since the turbulent velocities are of the order of 10 percent of the flow velocity, one might estimate that a system with 10 reticle lines across the field of view would satisfy the condition that the "blobs" remain intact across the field of view.

Formula (6) for the signal-to-shot noise power can also be applied for the reticle velocimeter. The illumination power in this case is supplied by the sun. The following example is given for comparison, but it is emphasized that the smoke property assumptions are rather arbitrary and may not be realistic.

Conditions:

Sunlight at 45°	=	Power density 300 W/m^2
Area Sampled on Smoke	=	.01 m^2 (.1 m x .1 m)
Number of Reticle Lines	=	10
Range	=	100 meters
Smoke Reflectivity	=	.1
Quantum Efficiency	=	.1
Smoke Velocity	=	40 m/sec
Receiver Aperture	=	.01 m^2
Contrast Ratio of Smoke, $\frac{I_{max} - I_{min}}{I_{ave}}$	=	.1
Number of "Blobs" Simultaneously in Field of View	=	100

The conditions preceding the last two give the following results:

Signal Frequency	=	4 KHz
Signal Bandwidth Δf	=	400 Hz
(Average Number of Detected Photons in Time Interval $\frac{1}{\Delta f}$)	=	6×10^7

The last two conditions give the modulation depth, $\bar{S}_1/S_o$, as .01, since there are approximately $\sqrt{100}$ "blobs" above or below the average "on" the fringes. Together with formula (6), these results yield

$$\frac{\text{Signal Power}}{\text{Shot Noise Power}} = \frac{1}{2} \cdot 6 \times 10^7 \cdot (.01)^2 = 3000 \quad .$$

This result suggests that the shot noise of detection may not pose much of a problem. This basically stems from the abundance of power provided by the sun and the narrow bandwidth Δf.

Whether artificial light (e.g., spotlights) could be used to permit night operation is not clear because of the large uncertainties in the above conditions.

Another source of noise, and quite possibly the primary noise source, is noise generated by the turbulence modulating the reflectivity of the smoke. Experiment appears to be the only approach to determine the magnitude of this noise source.

3.10 PRELIMINARY EXPERIMENTS WITH A RETICLE VELOCIMETER

A very rough set of experiments was done to explore the reticle velocimeter concept. A 2-inch diameter telescope objective was equipped with a photomultiplier and a reticle. The output of the photomultiplier went to an audio amplifier and a loudspeaker.

In a first experiment, a lambswool polishing wheel mounted in a hand electric drill served as simulated smoke. The wheel was placed in the sun, and visually would be described as a low contrast target. At 50 feet, the maximum space available, the speaker output had a clearly recognizable tone which moved up and down appropriately as the instrument was slowly scanned along a diameter of the wheel.

Indoor night experiments at a few feet with a dc tungsten lamp as illumination also performed similarly.

The performance of this type of instrument is independent of range under the condition that the angular field size does not change. This condition means that the object area sampled increases as the range is increased.

The instrument also performed well as a velocimeter for automobiles. At about 75 feet, the passing of each car yielded a distinct tone pulse, and differences in velocity were readily apparent to the ear. Car headlights at a distance of 2 miles at night gave a just detectable tone. The reticle spacing was such that the tone produced was actually too low for the pass band of the audio amplifier at this long range.

No smoke plumes were readily available in the Los Angeles area, but an attempt was made to use the velocimeter on a refinery burn-off flame. The attempt, done at night, was unsuccessful. The main reason was that at the nearest available distance to the flame (about 2000 feet), the field of view of the instrument was larger than the entire flame. It should have been small enough to sample only a small area near the mouth of the pipe. In consequence, the principal output consisted of noise from intensity fluctuations of the flame itself. Another possible reason for the failure with the flame may be that the flame propagation velocities are higher than the average translation velocity. Thus, the luminous structure is changing faster than the "blobs" can be swept across the reticle lines by the average translation. There is reason to expect smoke to be more coherent in this respect than a flame, due to the high flame propagation velocities. At times a crackling or frying noise was apparent, and visually corresponded to a "sparkle" in the flame.

In spite of the failure of the flame experiment, it is still felt that a properly designed experiment that examines a small area near the pipe's rim has some chance of success with flame and a good chance for success with smoke.

4. CONCLUSIONS

4.1 PORTABLE LASER VELOCIMETER

A portable laser velocimeter was designed and built to measure particle laden stack gas velocities based upon backscatter signals generated by the particulate as it passed through the region generated by two intersecting laser beams. Only limited testing of the instrument in a laboratory environment was accomplished due to cost and schedule constraints of the program. Sufficient work was done to satisfactorily demonstrate its operating range characteristics. Of significance in these tests was the sensitivity of the laser velocimeter to signals generated by backscattering of the incident laser beam on a smooth white paper disc. Application of the velocimeter to actual stack measurements, however, remains to be demonstrated.

Work on the present velocimeter has led to the conclusion that future models could be made even more compact and lighter weight. Utilization of a velocimeter in a fixed installation as a continuous stack gas velocity monitor would greatly simplify both the electronics and optical system. Unit costs in even limited production would be considerably reduced.

4.2 LONG RANGE VELOCIMETERS

This study examined the expected performance of three types of long-range smokestack velocimeters. The discussion attempted to expose the problems associated with each type of instrument, and to indicate what parameters are effective in optimizing the performance.

Definite conclusions are not possible because of unknown smoke properties. The reticle velocimeter appears attractive because of its extreme simplicity and resulting low cost. Its performance with smoke is still untested, but it has performed with a rotating wheel simulating "rigid" smoke. It should be explored further.

The two laser instruments each appear to require a one-watt argon laser in order to operate well at long distances.

The fringe velocimeter type appears to be the simpler to construct and can advantageously use a large collection aperture. Its actual performance will depend on the smoke properties; in particular, non-random clumping may assist its operation greatly. If the clumping does not

exist and the instrument is forced to operate on pure random particle distributions, the principal problem of the instrument then stems from the small magnitude of the intensity fluctuations, which in turn arise from the large number of particles simultaneously present in the probe volume.

The direct doppler instrument will only work at steep elevation angles due to turbulence in the smoke. This eliminates the really long range possibilities. The collection aperture is limited in size by coherence considerations. Multiple scattering may adversely affect its operation. Very high frequency electronic design is required for the direct doppler instrument, adding to the difficulty of constructing the direct doppler instrument.

More sophisticated instruments which give range resolution, and which function with very light particulate loading have not been considered in detail. It is felt that some actual experience should be acquired with a simple long-range system before embarking on the design of a more sophisticated system.

In interpreting the significance of the noise discussed in this report, it should be noted that the signal-to-noise ratios given are power ratios, as is customary practice. Note, however, that most display devices, such as meters and the oscilloscope deflection of a spectrum analyzer, are proportional to voltage. Thus, the ratio of deflections for signal and noise is given by the square root of the signal-power-to-noise-power ratio.

REFERENCES

1. A. E. Lennert, D. B. Brayton, F. L. Crosswy, W. H. Goethert, and H. T. Kalb, "Laser Technology in Aerodynamic Measurements," von Karman Institute for Fluid Dynamics Lecture Series 39, June 1971.

2. B. J. Matthews and H. Shelton, "Operation Manual - Portable Laser Velocimeter for Stack Velocity Measurements," TRW Report No. 20852-6001-TO-00, June 1972.

3. R.D. Ingebo, "Drop-Size Distributions for Impinging-Jet Breakup in Airstreams Simulating the Velocity Conditions in Rocket Combustors," NACA Technical Note 4222, March 1958.

APPENDIX A

SPECIFICATIONS FOR SPECTRA-PHYSICS MODEL 120 GAS LASER WITH MODEL 256 EXCITER

APPENDIX A

SPECIFICATIONS FOR SPECTRA-PHYSICS MODEL 120 GAS LASER WITH MODEL 256 EXCITER

Output Power: 5.0 mw @ 632.8 nm
Transverse Mode: TEM_{00}

Warm-up Time: > 3 mw 2 minutes after turn-on
> 5 mw 30 minutes after turn-on
Operating Temperature: 10 to 40°C
Long-Term Power Drift: < 5%

Altitude: Sea level to 10,000 feet

Beam Amplitude Noise (1-100 KHz): < 3%
Beam Amplitude Ripple (120 Hz): < 0.5%
Beam Polarization: Linear to better than 1 part per thousand
Plane of Polarization: Vertical, adjustable ±20°
Beam Diameter: 0.65 mm at $1/e^2$ points.
Beam Divergence: 1.7 milliradians at $1/e^2$ points

Resonator Configuration: Long Radius
Axial Mode Spacing: 385 MHz

Plasma Excitation: Direct current self-starting
Cable Length (Exciter to Laser): 8 feet (Extension sections available)
Dimensions: Model 120 Laser Head: 3.26" w x 3.66" h x 18.48" l
Model 256 Exciter: 7.25" w x 3.72" h x 9.88" l
Weight: Laser - 7½ lbs.
Exciter - 7½ lbs.
Input Power: 115/230v, 50/60Hz, 50va

APPENDIX B

LASER VELOCIMETER DRAWING LIST

APPENDIX B

Laser Velocimeter Drawing List

Drawing No.	Title
SK 1038-1	Velocimeter Probe
SK 1038-2	Support, Rack & Pinion Lense Assembly
SK 1038-3	Collar, Rack Pinion Assembly
SK 1038-5	Tube, Lense Holder Velocimeter Probe
SK 1038-6	Split Mirror, First Surface Support
SK 1038-7	Holder, Lense 30 MM dia.
SK 1038-9	Support, First Surface Mirror
SK 1038-10	Base, Sub Velocimeter Probe
SK 1038-11	Body, Beam Splitter
SK 1038-12	Laser Modification
SK 1038-13	Cover, Velocimeter
SK 1038-14	Panel, Velocimeter
SK 1038-15	Bracket, Grip Holding Tripod Support
SK 1038-17	Dial Face, Beam Splitter
SK 1038-18	Dial Face, Focus
SK 1038-21	Support, Laser
SK 1038-22	Support, Laser
SK 1038-31	Collar, Front Rack & Pinion
SK 1038-32	Collar, Rear Rack & Pinion
SK 1038-33	Support, Collar
SK 1038-34	Gear, Pinion & Shaft, Collar
SK 1038-35	Bearing, Tube, Lense Holder
SK 1038-51	Nut, Lense Holder Velocimeter Probe
SK 1038-52	Washer, Lense Holder Velocimeter Probe
SK 1038-53	Rack, Tube Lense Holder
SK 1038-61	Strap, Split Mirror
SK 1038-62	Split Mirror First Surface
SK 1038-71	Nut, Lense Holder 30 MM Dia.
SK 1038-72	Washer, Lense Holder 30 MM Dia.

Drawing No.	Title
SK 1038-91	Strap, Support First Surface Mirror
SK 1038-92	Mirror, First Surface
SK 1038-101	Spacer, Sub Base
SK 1038-102	Rubber Mount Assembly
SK 1038-111	Pawl, Beam Splitter Velocimeter
SK 1038-112	Link, Beam Splitter Velocimeter
SK 1038-113	Shaft, Beam Splitter Velocimeter
SK 1038-114	Slide, Prism Beam Splitter
SK 1038-115	Slide, Mirror First Surface Beam Splitter
SK 1038-116	Holder, First Surface Mirror Beam Splitter
SK 1038-117	Plate, Body, Beam Splitter
SK 1038-118	Gib, Vee Slide Beam Splitter
SK 1038-119	Gib Spring, Vee Slide, Beam Splitter
SK 1038-131	Window, Lense Focus
SK 1038-141	Focus Dial Window
SK 1038-142	Beam Dial Window
SK 1038-151	Support, Tripod
SK 1038-171	Post, Dial Beam Splitter
SK 1038-172	Pointer, Dial Beam Splitter
SK 1038-181	Pointer, Holder
SK 1038-182	Pointer, Focus
SK 1038-1110	Spring, Vee Slide, Beam Splitter
SK 1038-1111	Spring Drag, Beam Splitter Adjustment